

Enhancement of Optical Absorption in Amorphous Silicon Solar Cells Using Multilayer Nanoparticle Arrays and By Up-Conversion of Light

Himanshu

A Dissertation Submitted to
Indian Institute of Technology Hyderabad
In Partial Fulfillment of the Requirements for
The Degree of Master of Technology



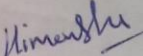
भारतीय प्रौद्योगिकी संस्थान हैदराबाद
Indian Institute of Technology Hyderabad

Department of Electrical Engineering

June, 2016

Declaration

I declare that this written submission represents my ideas in my own words, and where others' ideas or words have been included, I have adequately cited and referenced the original sources. I also declare that I have adhered to all principles of academic honesty and integrity and have not misrepresented or fabricated or falsified any idea/data/fact/source in my submission. I understand that any violation of the above will be a cause for disciplinary action by the Institute and can also evoke penal action from the sources that have thus not been properly cited, or from whom proper permission has not been taken when needed.


Himanshu

EE14MTECH11016

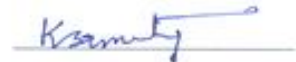
Approval Sheet

This thesis entitled **Enhancement of Optical Absorption in Amorphous Silicon Solar Cells Using Multilayer Nanoparticle Arrays and By Up-Conversion of Light** – by **Himanshu** is approved for the degree of Master of Technology/ Doctor of Philosophy from IIT Hyderabad.



Dr. GVV Sharma

- Department of Electrical Engineering
Examiner



Dr. Sri Rama Murty Kodukula

- Department of Electrical Engineering
Examiner



- Dr. Siva Rama Krishna Vanjari

- Department of Electrical Engineering
Adviser



Dr. Pankaj Kolhe

- Department of Mechanical Aero Space Engineering
Chairman
-

Acknowledgements

Success does not come easy. One has to put in a lot of hard work and in this process one takes all the encouraging and helping hands. Words often fail to express one's inner feelings of the gratitude to his benefactors and mentors. Firstly, I thank the almighty for giving me all his blessings that helped in the successful completion of this report. I would like to express my heartiest concern to **Dr. Siva Rama Krishna Vanjari** for his guidance and for praiseworthy attitude and honest support during this period.

I am also thankful to **Prof. Mohammed Zafar Ali Khan**, Head, Electrical department, for his new ideas and long sightedness that helped throughout the thesis work.

Last but not the least, I would like to thanks my family and friends who were there when I need them. At the end, I humbly offer my thanks to all those people who have contributed in the completion of this report. The entire experience has not only increased my knowledge and potential but also inculcated in me the desire to learn more and aim higher.

Himanshu

Dedicated to

To my beloved parents and family for their support and my friends.

Abstract

Recently, thin-film solar cells enhanced with plasmonic nanoparticles have attracted much attention of the scientific community. To improve the performance of such cells, an optimization of the nanoparticle parameters such as size, surface coverage and material is performed. Also it is found out that lanthanides along with host material can be used for upconversion process which further enhances the absorption efficiency for solar cells. Based on this optimization, the role of surface plasmons and upconversion process is discussed and analyzed with respect to optical absorption of the photoactive layer.

This thesis focuses on the use of lanthanide ions for spectral conversion in solar cells. The main energy loss in the conversion of solar energy to electricity is related to the so-called spectral mismatch: low energy photons are not absorbed by a solar cell while high energy photons are not used efficiently. To reduce the spectral mismatch losses both upconversion and downconversion are viable options. In the case of upconversion two low energy infrared photons that cannot be absorbed by the solar cell, are added up to give one high energy photon that can be absorbed. In the case of downconversion one high energy photon is split into two lower energy photons that can both be absorbed by the solar cell. The rich and unique energy level structure arising from the 4fⁿ inner shell configuration of the trivalent lanthanide ions gives a variety of options for efficient up- and downconversion. Here upconversion process has been used for improving solar cell efficiency.

The light absorption efficiency is enhanced in the lower wavelengths by a nanoparticle array on the surface and in the higher wavelengths by another nanoparticle array and lanthanide layer embedded in the active region. The efficiency at intermediate wavelengths is enhanced by the simultaneous resonance from both nanoparticle layers. We optimize this design by tuning the radius of particles in both arrays, the period of the array, the distance between the two arrays and the thickness of lanthanide layer. The optimization results in a total quantum efficiency of 60.99% for a 0.3 μm thick a-Si substrate.

Contents

Declaration.....	ii
Approval Sheet	iii
Acknowledgements.....	iv
Abstract.....	vi
1 Introduction.....	1
1.1 Motivation.....	6
1.2 Aim and objectives of the thesis	7
1.3 Thesis outline.....	7
2 Literature Survey and Theory.....	8
2.1 Plasmon nanoparticles	8
2.2 Surface plasmon resonance.....	11
2.3 Plasmonic solar cells.....	12
3 Photon Up-conversion	14
3.1 Spectral conversion.....	14
3.2 Up-conversion.....	16
3.3 Rare earth doped up-converter materials	17
3.3.1 Excited state absorption (ESA)	18
3.3.2 Energy transfer upconversion (ETA)	18
3.3.3 Photon avalanche (PA).....	18
3.3.4 Energy migration-mediated upconversion	19
3.4 Host materials	19
4 Ag as nanoparticle material	22
5 Proposed solar cell design	27
5.1 Proposed design	30
5.2 Results	31
6 Design parameters and their effects.....	36
6.1 Effect of nanoparticle radii	36
6.1.1 Effect of surface layer nanoparticle.....	37
6.1.2 Effect of bulk layer nanoparticle.....	38
6.2 Effect of particle layer separation.....	39

6.3	Effect of vertical alignment of particle layers.....	41
7	Conclusion	43
	References.....	44

Chapter 1

Introduction

In recent years there has been a significant, resurgent interest in renewable energy sources. This has been partially motivated by the increase in oil prices worldwide as a result of geopolitical and economic factors, and the general concern associated with global warming that is exacerbated by the emission of greenhouse gases during the production of primary power by conventional means. While many technologies are being considered to supplement oil as a primary energy source, renewable energy sources are seen as the key to long-term weaning of industrialized economies from strict reliance on oil, coal, and natural gas. These include wind, fuel cells, solar cells, geothermal, biofuels, etc. Solar energy conversion is perhaps the most appealing of all these solutions, since the energy source is readily available [1,2].

Sustainable energy production based on the direct conversion of energy radiated from the sun into useable forms like heat or electricity is expected to gain importance since it may be the only renewable source capable of generating sufficient energy to meet the long-term worldwide energy demand. Solar energy utilization requires effective means of capture and conversion of the solar radiation, and storage of the acquired energy. The capacity of photovoltaic cells to convert sunlight into electricity makes them prime candidates for effective large-scale capture and conversion of solar energy, but at present the contribution of photovoltaic energy is limited due to its relatively high cost per kilowatt-hour and poor absorption efficiency. A reduction in price may be achieved by either lowering the production cost or increasing the conversion efficiency [3].

The concept of converting light to electricity was first introduced with the discovery of the photovoltaic (PV) effect by Edmond Becquerel in 1839 [4]. However, the first commercially viable demonstration of a solar cell did not occur until over 100 years later, with the invention of the crystalline Si-based cell first revealed to the world by researchers at Bell Labs in 1954 [5]. Silicon is the material of choice for photovoltaic applications due to its low cost,

abundance in nature, nontoxicity, long-term stability, and well established technology. The first Si cell had an efficiency of 4% and since then researchers have been attempting to demonstrate, and companies to commercialize, solar cells with high conversion efficiency and low manufacturing cost. In the ensuing 50 years, Si cells have been demonstrated with an efficiency of nearly 25% [6], very close to the theoretical limit (given by Shockley–Queisser limit) for a single junction under one sun illumination of 31% [7, 8].

Shockley–Queisser limit

The Shockley–Queisser limit or Shockley Queisser Efficiency Limit refers to the maximum theoretical efficiency of a solar cell using a single p-n junction to collect power from the cell. It was first calculated by William Shockley and Hans-Joachim Queisser at Shockley Semiconductor in 1961. The limit is one of the most fundamental to solar energy production, and is considered to be one of the most important contributions in the field.

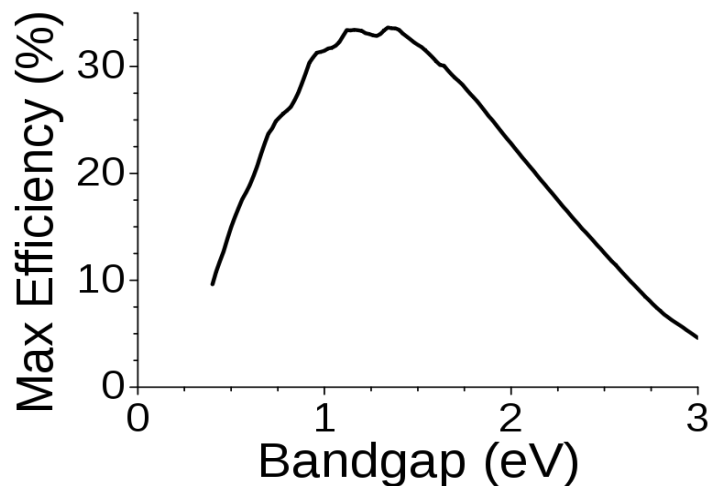


Fig 1.1: The Shockley-Queisser limit for the maximum possible efficiency of a solar cell as a function of band-gap

The limit places maximum solar conversion efficiency around 33.7% assuming a single p-n junction with a band gap of 1.34 eV (using an AM 1.5 solar spectrum). That is, of all the power contained in sunlight falling on an ideal solar cell (about 1000 W/m²), only 33.7% of that could ever be turned into electricity (337 W/m²). The most popular solar cell material, silicon, has a less favorable band gap of 1.1 eV, resulting in a maximum efficiency of about 32%. Modern commercial mono-crystalline solar cells produce about 24% conversion efficiency, the losses due largely to practical concerns like reflection off the front surface and

light blockage from the thin wires on its surface. The Shockley–Queisser limit only applies to cells with a single p-n junction; cells with multiple layers can outperform this limit.

Thin film solar cells

To make electricity from photovoltaics competitive with fossil fuel technologies, the price needs to be reduced significantly. Currently 90 % of the solar cell market is based on crystalline silicon wafers, with thicknesses of 200-300 μm . Around 40% of the cost of a solar module made from crystalline silicon is the cost of the silicon wafers. Because of this, there has been a great deal of research on thin-film solar cells over the past years.

Thin film solar cells have become a potential alternative to traditional crystalline silicon solar cells due to lower manufacturing costs, better flexibility, easy preparation, durability and shorter energy payback period. A better understanding of the underlying physics and the availability of mature fabrication technology makes amorphous silicon the preferred choice for thin film photovoltaic cells [9]. Thin-film solar cells have thicknesses usually in the range 1-2 μm , and are deposited on cheap foreign substrates such as glass, plastic, stainless steel or metal for mechanical support. They are made from a variety of semiconductors including cadmium telluride as well as amorphous and polycrystalline silicon. A major limitation in all thin film solar cell technologies is that their absorbance of near-bandgap light is ineffective, in particular for the indirect-bandgap semiconductor silicon [2]. Also, the efficiencies of such silicon thin-film cells at the moment are low compared to wafer-based silicon cells because of the relatively poor light absorption, as well as high bulk and surface recombination. Therefore, structuring the solar cell so that light is trapped inside, in order to increase the absorbance, is very important.

Light trapping mechanisms

Because silicon is a weak absorber, light-trapping is also used in wafer-based cells. For wafer cells, pyramids of small size are etched into the surface. For thin-film cells with thicknesses in the micron range, surface texturing with these dimensions is not suitable, so new methods must be found.

It is possible to achieve light-trapping by forming a wavelength-scale texture on the substrate and then depositing the thin-film solar cell on top, and large increases in photocurrent have been achieved in this way [10, 11]. However, a rough semiconductor surface results in increased surface recombination.

A new method for increasing the light absorption that has emerged recently is the use of scattering from noble metal nanoparticles excited at their surface plasmon resonance [2]. Advancements in the field of plasmonics have shown the promising capability of metallic Nano structures to improve light-trapping in sub wavelength solar cells. Nanostructured metallic films can maintain surface Plasmon polaritons, a special kind of plasma surface waves, that able to concentrate light into sub wavelength scale near the surface. In addition, metallic nanoparticles deposited on top of cells also can improve photo electron generation in the active region. They enable very efficient scattering of light at high scattering angles that makes it possible to couple the scattered light with trapped waveguide modes of the photo active layer and improve the light-trapping over a broad range of the solar spectrum.

Major advantage of using plasmonics for light trapping process is that during fabrication metal nanoparticles are deposited at last stage of fabrication process hence almost entire fabrication process can be carried out in same environment of processing conditions without compromising the quality of either metal or surface. The cell structure is independent of the surface plasmons implying that the optical properties of the surface plasmons are decoupled from the electrical properties of the solar cell hence can be optimized independently. The resonant natures of plasmonic enhancements make the nanoparticles a very efficient and flexible tool for solar cell applications, which can be used to manipulate the light trapping and energy conversion efficiency.

Efficiency improvement of solar cells

The efficiency of solar cells can be improved either by increasing the light absorption efficiency or by increasing the minority carrier life time. In order to increase the light absorption, it becomes necessary to incorporate light trapping mechanisms in solar cells. Nanoparticles exhibit the phenomenon of surface plasmon resonance when illuminated with light of suitable frequency [12-14]. Near the plasmon resonance frequency, metallic nanoparticles strongly scatter light incident on it. This scattering effect is the result of the collective oscillations of electrons to re-radiate electromagnetic radiation [15]. When placed on the surface of silicon substrate, metallic nanoparticles scatter light preferentially into it due to the high refractive index of silicon [16]. The particles also scatter the incident light at an angle, thereby increasing the path length of photons within the silicon substrate. As a result, the optical thickness of the active region increases, thereby allowing the semiconductor substrate to absorb higher levels of electromagnetic radiation [17].

Researchers have explored the possibility of placing nanoparticles on the surface [18, 13, 19], rear [20] and within the active region [21] of thin film solar cells. Multiple arrays of nanostructures placed either on the front, rear or both are used to further enhance the absorption efficiency [22-24]. The phenomenon of energy transfer between discrete nanostructures located at the surface and active region of a solar cell is used to control the flow of energy and improve absorption efficiency [25]. In these cases, enhancing the quantum efficiency has been considered over limited bands of wavelengths. Also, a loss in performance is possible if the metallic nanoparticles are introduced in the bulk due to increased recombination [26, 27]. However, it is possible to prevent the metallic nanoparticles from acting as recombination centers either by using room temperature processes such as microcontact printing [28] or by passivating it with a dielectric coating [21]. Motivated by these facts, we enhance the light absorption efficiency of a thin film a-Si solar cell by placing periodic arrays of silver nanoparticles at the surface and within the active region of the cell. The surface and bulk layer of nanoparticles enhances the absorption of lower and higher wavelengths respectively. In addition the absorption of light within the substrate is further enhanced by the simultaneous resonance from the surface and bulk layers at intermediate wavelengths. Due to the multiple and high-angle scattering from both the layers of nanoparticles, the effective optical path length of light increases inside the cell. This results in several fold increase in the optical thickness of the active region without increasing the physical thickness [17].

Upconversion

One of the prominent research areas of nanomaterials for photovoltaics involves spectral conversion. Modification of the spectrum requires down- and/or upconversion or downshifting of the spectrum, meaning that the energy of photons is modified to either lower (down) or higher (up) energy. Nanostructures such as quantum dots, luminescent dye molecules, and lanthanide-doped glasses are capable of absorbing photons at a certain wavelength and emitting photons at a different (shorter or longer) wavelength [29].

The band-gap of amorphous Si is larger than that of c-Si at about 1.75 eV, which confines it to absorb NIR light shorter than 700 nm. This means that upconverting materials with absorption above 700 nm should be appealing for uses in amorphous Si solar cells to circumvent the transmission loss.

Zhang [30] investigated the use of NaYF₄:18% Yb³⁺, 2% Er³⁺ nanocrystals as upconverter in an amorphous Si solar cell to enhance the power conversion efficiency. This kind of upconverter shows visible emissions at around 655 nm (red), 525 nm and 540 nm (green) after absorbing light at 980 nm.

1.1 Motivation

As solar energy seems to be only renewable source of energy that is easily available to full fill our future needs of energy, research is to be done to reduce the cost of the commercially available solar cells and to improve the efficiency of solar cells so that more amount of energy can be harvested. Figure below shows the spectrum of solar radiation received on earth:

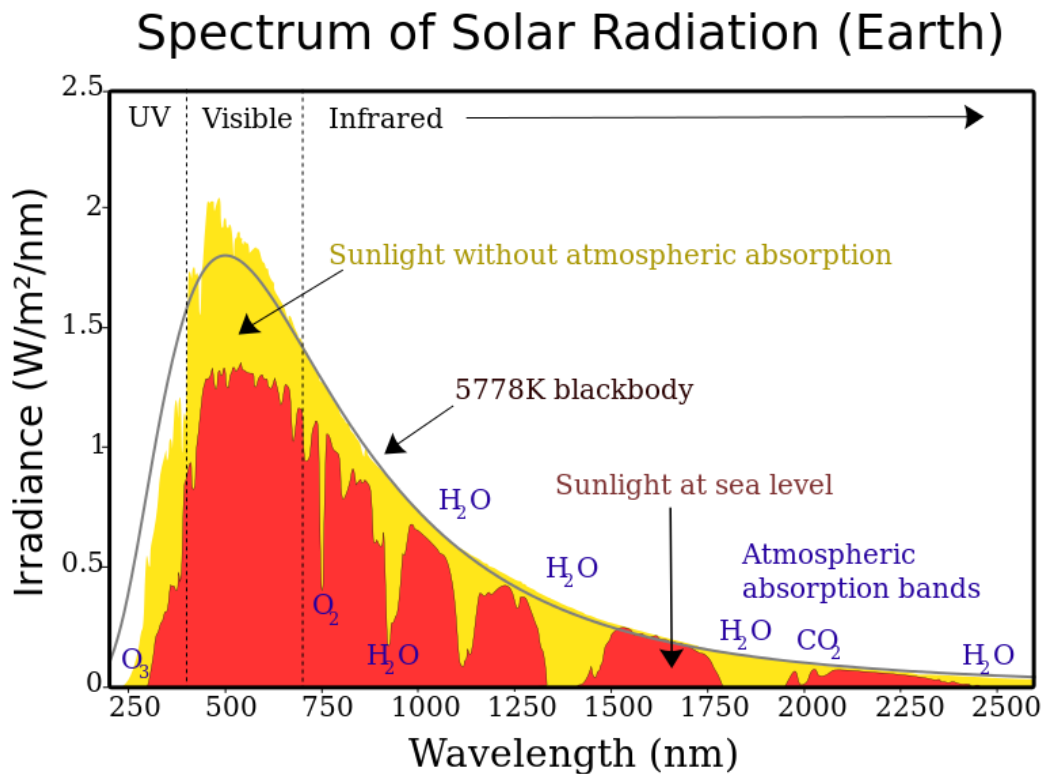


Fig 1.2: solar radiation spectrum

Most of the solar cells available today absorb light from the visible region of the solar spectrum, and this range is limited because of the material band gap limitations. Most widely used material for solar cells i.e. c-Si has a band gap of ~1.1eV which restricts its absorption limit to a wavelength of ~1100 nm max. Because of this almost 40% of the solar power that

comes to earth is entirely wasted. This absorption range is to be broadened to have better efficiency for solar cells.

1.2 Aim and objectives of the thesis

Main aim of thesis is to enhance the solar cell efficiency by using light trapping mechanisms in the visible and in the IR region by figuring out the broad spectrum characteristics of scattering and absorption from a Silicon substrate with metallic Nano structures embedded on it. The simulations address the behavior of scattered and absorbed power densities for broad spectrum of un-polarized electromagnetic waves. The change in characteristics of scattering and absorption with the angle of incidence is also addressed. The Nano structures are optimized in order to maximize the absorption by the Si substrate. Also we will try to improve solar cell efficiency using up-conversion process which is carried out using lanthanide ions.

1.3 Thesis outline

The remainder of the thesis is organized as follows:

- *Chapter 2* provides background knowledge and concepts for the surface plasmon resonance.
- *Chapter 3* explains the concept of photon upconversion process and covers all the properties associated with upconverter materials.
- *Chapter 4* gives an insight of why silver nanoparticles are best suitable for the given solar cells.
- *Chapter 5* explains the proposed solar cell design, design parameters and results.
- *Chapter 6* describes all the parameters and their variation effects on the solar cell efficiency.
- *Chapter 7* concludes the thesis.

Chapter 2

Literature Survey and Theory

2.1 Plasmon nanoparticles

Plasmonic nanoparticles are particles whose electron density can couple with electromagnetic radiation of wavelengths that are far larger than the particle due to the nature of the dielectric-metal interface between the medium and the particles: unlike in a pure metal where there is a maximum limit on what size wavelength can be effectively coupled based on the material size.

What differentiates these particles from normal surface plasmons is that plasmonic nanoparticles also exhibit interesting scattering, absorbance and coupling properties based on their geometries and relative positions. These unique properties have made them a focus of research in many applications including solar cells, spectroscopy, signal enhancement for imaging, and cancer treatment.

Plasmons are the oscillations of free electrons that are the consequence of the formation of a dipole in the material due to electromagnetic waves. The electrons migrate in the material to restore its initial state; however, the light waves oscillate, leading to a constant shift in the dipole that forces the electrons to oscillate at the same frequency as the light. This coupling only occurs when the frequency of the light is equal to or less than the plasma frequency and is greatest at the plasma frequency that is therefore called the resonant frequency. The scattering and absorbance cross-sections describe the intensity of a given frequency to be scattered or absorbed. Many fabrication processes exist for fabricating such nanoparticles, depending on the desired size and geometry.

The resonant behavior of localized surface plasmons are restricted to a limited range of frequencies determined by the size and shape of the particles, dielectric functions of the involved media, and the electromagnetic interaction between them [31]. When the frequency

of light incident on the nanoparticles match the natural frequency of the oscillating surface electrons, the phenomenon of surface plasmon resonance is established [32].

For particles with diameters well below the wavelength of light, a point dipole model describes the absorption and scattering of light well. The scattering and absorption cross-sections are given by:

$$C_{scat} = \frac{1}{6\pi} \left(\frac{2\pi}{\lambda} \right)^4 |\alpha|^2, \quad C_{abs} = \frac{2\pi}{\lambda} \text{Im}[\alpha]$$

$$\alpha = 3V \left[\frac{\epsilon_p / \epsilon_m - 1}{\epsilon_p / \epsilon_m + 2} \right]$$

Where α is the polarizability of the particle.

Here V is the particle volume, ϵ_p is the dielectric function of the particle and ϵ_m is the dielectric function of the embedding medium. We can see that when $\epsilon_p = -\epsilon_m$ the particle polarizability will become very large. This is known as the surface plasmon resonance. At the surface plasmon resonance the scattering cross-section can well exceed the geometrical cross section of the particle. For example, at resonance a small silver nanoparticle in air has a scattering cross-section that is around ten times the cross sectional area of the particle. In such a case, to first-order, a substrate covered with a 10 % areal density of particles could fully absorb and scatter the incident light. For light trapping it is important that scattering is more efficient than absorption.

The size dependent dielectric function the particle $\epsilon(\omega, D)$ is given by, [31]

$$\epsilon(\omega, D) = \epsilon_{IB} + \left(1 - \frac{\omega_p^2}{\omega^2 + i\omega\gamma(D)} \right)$$

where D is the diameter of the particle and $i = \sqrt{-1}$. The size independent first term ϵ_{IB} is due to inter-band transitions. The second term is the Drude-Sommerfeld free electron term which contains the bulk plasmon frequency ω_p , given by $\omega_p^2 = Ne^2/m\epsilon_0$ where N is the density

of free electrons, e is the electronic charge, m is the effective mass of an electron and ϵ_0 is the free-space dielectric constant, and the size-dependent damping constant γ ; [31]

$$\gamma(D) = \gamma_0 + 2 \left(\frac{Av_F}{D} \right)$$

where γ_0 is the bulk damping rate and v_F is the Fermi velocity of the electrons. A is a dimensionless size parameter which accounts for the additional surface damping terms, such as the inelastic collisions between electrons and chemical interface damping. Inelastic collisions shorten the mean free path of the electrons when nanoparticle size decreases. Chemical interface damping occurs in embedded nanoparticles, where the fast energy transfer between the particle and its surroundings results in the loss of phase coherence of the collective electron oscillation.

The particle polarizability becomes large when $\epsilon_p = -2\epsilon_m$, and this effect is called surface plasmon resonance. At resonance the particle scattering cross-section area, C_{scat} , a parameter that determines the extent to which scattering of light occurs, is several times the geometric cross section of the particle [15].

$$C_{scat} = \frac{1}{6\pi} \left(\frac{2\pi}{\lambda} \right)^4 |\alpha|^2$$

where λ is the wavelength of the incident light. For particles with diameter in the range of a few nanometers, scattering is also accompanied by absorption. As particle diameter increases to around 100 nanometers, the scattering effect strongly outweighs the absorption by the particle [33]. Also, the resonance is accompanied by another process, namely dynamic depolarization [34]. As size increases, the oscillation of the conduction electrons at resonance goes out of phase, resulting in a red shift of the particle resonance. The increase in size also results in higher radiation damping, which results in the broadening of the range of frequencies at which resonance occurs [35, 36]. The surface plasmon resonance can be tuned to a large extent either by coating or sandwiching the nanostructure with a dielectric medium. The medium can markedly enhance the red shift of the central wavelength and consequently obtain a wide tunable range at higher wavelengths [37]. Both red shifting and broadening of resonance frequencies are advantageous for the solar cell [33].

2.2 Surface plasmon resonance

Surface plasmons are those plasmons that are confined to surfaces and that interact strongly with light resulting in a polariton. They occur at the interface of a vacuum or material. Surface plasmon resonance (SPR) can be described as the resonant, collective oscillation of valence electrons in a solid stimulated by incident light. The resonance condition is established when the frequency of light photons matches the natural frequency of surface electrons oscillating against the restoring force of positive nuclei. SPR in nanometer-sized structures is called localized surface plasmon resonance. SPR is the basis of many standard tools for measuring adsorption of material onto the surface of metal nanoparticles. It is the fundamental principle behind many color-based biosensor applications and different lab-on-a-chip sensors.

Localized surface plasmon resonances are collective electron charge oscillations in metallic nanoparticles that are excited by light. They exhibit enhanced near-field amplitude at the resonance wavelength. This field is highly localized at the nanoparticle and decays rapidly away from the nanoparticle/dielectric interface into the dielectric background, though far-field scattering by the particle is also enhanced by the resonance. Light intensity enhancement is a very important aspect of localized surface plasmon resonances and localization means the localized surface plasmon resonance has very high spatial resolution (subwavelength), limited only by the size of nanoparticles. Because of the enhanced field amplitude, effects that depend on the amplitude such as magneto-optical effect are also enhanced by localized surface plasmon resonances

Understanding the basic mechanism of localized surface plasmon resonance and various parameters affecting it is necessary to engineer the nanoparticles for light trapping applications in solar cells [5]. The electromagnetic properties of metal particles have been known for a long time but there has been renewed interest in recent years following the development of new nanofabrication techniques which makes it easy to fabricate these nanostructures. Localized surface plasmons are collective oscillations of the conduction electrons in metal particles. Movement of the conduction electrons upon excitation with incident light leads to a buildup of polarization charges on the particle surface. This acts as a restoring force, allowing a resonance to occur at a particular frequency, which is termed the dipole surface plasmon resonance frequency [38].

For the commonly used metals, such as silver, gold, and copper, the surface plasmon resonances usually lie in the visible range and provide a very efficient way to control and tune the spectral response of the photoactive layer for the incident sunlight. A major benefit of plasmonic light trapping lies in the fact that the metal nanoparticles can be deposited at the final stage of the device fabrication process without the need to change any processing conditions or compromise the material or surface quality. An added advantage is that the optical properties of the surface plasmons are decoupled from the electrical properties of the solar cell hence can be optimized independent of the cell structure. The resonant natures of plasmonic enhancements make the nanoparticles a very efficient and flexible tool for solar cell applications, which can be used to manipulate the light trapping and energy conversion efficiency.

2.3 Plasmonic solar cells

A Plasmonic solar cell is a type of thin film solar cell that converts light into electricity with the assistance of plasmons. They are typically less than 2 μm thick and theoretically could be as thin as 100 nm. They can use substrates which are cheaper than silicon, such as glass, plastic or steel. One of the challenges for thin film solar cells is that they do not absorb as much light as thicker solar cells made with materials with the same absorption coefficient. Methods for light trapping are important for thin film solar cells. Plasmonic cells improve absorption by scattering light using metal nano-particles excited at their surface plasmon resonance. This allows light to be absorbed more directly without the relatively thick absorber layer required in other types of thin-film solar cells. However, this type of solar cell also normally demands a thin transparent conducting oxide to function for realistic photovoltaic absorber thickness and now there are methods available that allow high conductivity while maintaining high optical transmission of the transparent conducting oxide.

There are currently three different generations of solar cells. The first generation (those in the market today) are made with crystalline semiconductor wafers, typically silicon. Current solar cells trap light by creating pyramids on the surface which have dimensions bigger than most thin film solar cells. Making the surface of the substrate rough (typically by growing SnO_2 or ZnO on surface) with dimensions on the order of the incoming wavelengths and depositing the solar cell on top has been explored. This method increases the photocurrent but the thin film solar cell would then have poor material quality.

The second generation solar cells are based on thin film technologies such as those presented in this thesis. These solar cells focus on lowering the amount of material used as well as increasing the energy production.

A common design is to deposit metal nano-particles on the top surface of the thin film solar cell. When light hits these metal nano-particles at their surface plasmon resonance, the light is scattered in many different directions. This allows light to travel along the SC and bounce between the substrate and the nano-particles enabling the solar cell to absorb more light.

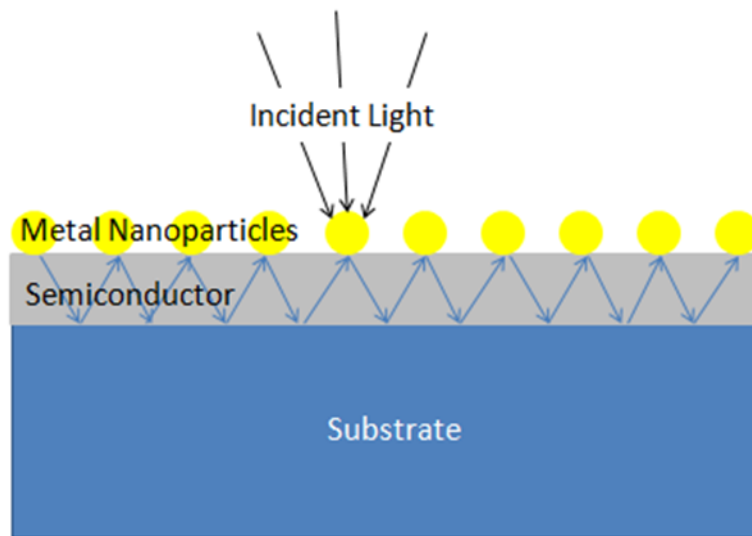


Fig 2.1: Basic design of plasmonic solar cell

Recent advances in the rapidly emerging field of plasmonics have shown the promising capability of metallic nanostructures to improve light-trapping in sub wavelength solar cells. Nano-structured metallic films can maintain surface Plasmon polaritons, a special kind of plasma surface waves, that able to concentrate light into subwavelength scale near the surface. Thus, coupling of the incident sunlight with the surface Plasmon polaritons can improve the light-trapping and absorption of thin-film solar cells. In addition, metallic nanoparticles deposited on top of cells also can improve photoelectron generation in the active region. They enable very efficient scattering of light at high scattering angles that makes it possible to couple the scattered light with trapped waveguide modes of the photoactive layer and improve the light-trapping over a broad range of the solar spectrum.

Chapter 3

Photon Up-conversion

Photovoltaic cells are able to convert sunlight into electricity, providing enough of the most abundant and cleanest energy to cover our energy needs. However, the efficiency of current photovoltaics is significantly impeded by the transmission loss of sub-band-gap photons. Photon up-conversion is a promising route to circumvent this problem by converting these transmitted sub-band-gap photons into above-band-gap light, where solar cells typically have high quantum efficiency [29].

The possibility to tune chemical and physical properties in nano-sized materials has a strong impact on a variety of technologies, including photovoltaics. One of the prominent research areas of nanomaterials for photovoltaics involves spectral conversion. Modification of the spectrum requires down- and/or up-conversion or downshifting of the spectrum, meaning that the energy of photons is modified to either lower (down) or higher (up) energy. Nanostructures such as quantum dots, luminescent dye molecules, and lanthanide-doped glasses are capable of absorbing photons at a certain wavelength and emitting photons at a different (shorter or longer) wavelength.

3.1 Spectral conversion

Spectral conversion aims at modifying the incident solar spectrum such that a better match is obtained with the wavelength-dependent conversion efficiency of the solar cell. Its advantage is that it can be applied to existing solar cells and that optimization of the solar cell and spectral converter can be done separately [39].

Different types of spectral conversion can be distinguished:

1. Up-conversion, in which two low-energy (sub-bandgap) photons are combined to give one high-energy photon

2. Downshifting or luminescence, in which one high-energy photon is transformed into one lower energy photon and
3. Down-conversion or quantum cutting, in which one high-energy photon is transformed into two lower energy photons.

Downshifting can give an efficiency increase by shifting photons to a spectral region where the solar cell has a higher quantum efficiency i.e. basically improving the blue response of the solar cell, and improvements of up to 10% relative efficiency increase have been predicted [40]. Up and down conversion, however, are predicted to be able to raise the efficiency above the SQ limit [41, 42]. For example, Richards [43] has shown for crystalline silicon (c-Si) that the potential relative gain in efficiency could be 32% and 35% for down-conversion and upconversion respectively, both calculated for the standard 1,000-W/m² air mass (AM) 1.5 solar spectrum.

The usefulness of down and up conversion and downshifting depends on the incident spectrum and intensity. Spectral conditions for solar cells vary from AM0 (extraterrestrial) via AM1 (equator, summer and winter solstice) to AM10 (sunrise, sunset). The weighted average photon energy (APE) [44] can be used to parameterize this; the APE (using the range 300 to 1,400 nm) of AM1.5G is 1.674 eV, while the APE of AM0 and AM10 are 1.697 and 1.307 eV, respectively. Further, overcast skies cause higher scattering leading to diffuse spectra, which are blue-rich, e.g., the APE of the AM1.5 diffuse spectrum is calculated to be 2.005 eV, indeed much larger than the APE of the AM1.5 direct spectrum of 1.610 eV. As down-conversion and downshifting effectively red-shift spectra, the more relative energy an incident spectrum contains in the blue part of the spectrum (high APE), the more gain can be expected [43, 45]. Application of down-conversion layers will therefore be more beneficial for regions with high diffuse irradiation fraction, such as Northwestern Europe, where this fraction can be 50% or higher. In contrast, solar cells with upconversion layers will be performing well in countries with high direct irradiation fractions or in early morning and evening due to the high air mass resulting in low APE, albeit that the non-linear response to intensity may be limiting. Up- and down-conversion layers could be combined on the same solar cell to overcome regionally dependent efficiencies. Optimization of either up- or down conversion layers could be very effective if the solar cell bandgap is a free design parameter [8].

3.2 Up-conversion

Upconversion was initially related to the development of infrared (IR) detectors: IR photons would be detected through sequential absorption, as would be possible by the arrangement of energy levels of a solid. However, as Auzel pointed out, the essential role of energy transfer was only recognized nearly 20 years later [46]. Several types of upconversion mechanism exist, of which energy transfer upconversion mechanism is the most efficient; it involves energy transfer from an excited ion, named sensitizer, to a neighboring ion, named activator [46]. Others are two-step absorption, being a ground-state absorption followed by an excited-state absorption, and second-harmonic generation. The latter mechanism requires extremely high intensities, of about 10^{10} times the sun's intensity on a sunny day, to take place [47] and can therefore be ruled out as a viable mechanism for solar cell enhancement.

Three types of upconversion methods can be used to cover entire spectrum from Visible to near infra-red (from 700 nm to 2500 nm) [29]:

1. For wavelength $> 800\text{nm}$, **Rare earth doped metals (RED-UC)** i.e. Lanthanides (from atomic number 57 to 71). The abundant electronic states of trivalent lanthanide ions enable upconverting a range of IR wavelengths by selecting varied types of rare earth ions [48, 49].

2. For wavelength $< 800\text{nm}$, **Triplet-triplet annihilation upconversion (TTA-UC)**: Two nearby acceptor (annihilator) molecules in the triplet states collide with each other, and results in one acceptor molecule being excited to the higher singlet state, while the other one returns to the ground singlet state. A radiative decay from the generated singlet excited state of the acceptor produces an upconverted fluorescence, which is called triplet-triplet annihilation (TTA) upconversion.

3. For wavelength $< 800\text{nm}$, **Quantum nanostructure (QN-UC)**: using a compound semiconductor nanocrystal, which incorporates two quantum dots with different bandgaps separated by a tunneling barrier. Upconversion occurs by excitation of an electron in the lower energy transition, followed by intra-band absorption of the hole, allowing it to cross the barrier to a higher energy state.

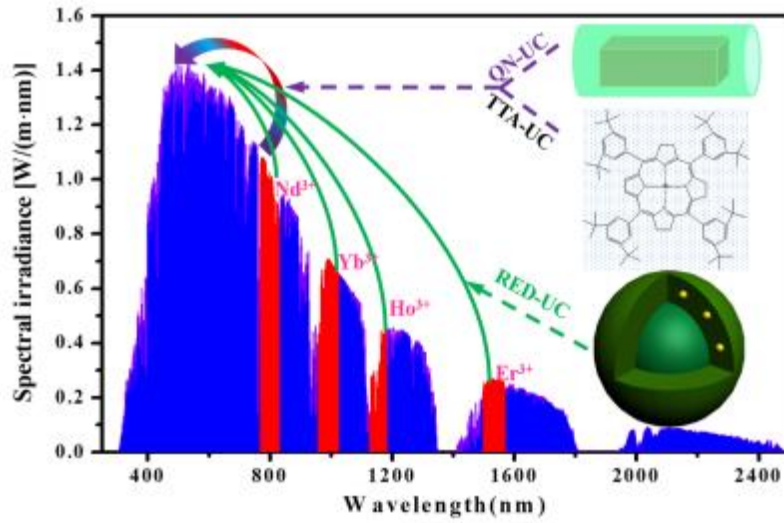


Fig 3.1: The absorption and emission range of three types of upconversion materials in reference to AM 1.5 spectrum (QN-UC (purple): upconversion in quantum nanostructures; TTA-UC (purple): triplet-triplet annihilation upconversion; RED-UC (green): Rare-earth-doped upconversion materials)[9].

3.3 Rare earth doped up-converter materials

The rare-earth family is comprised of 17 elements, which includes 15 lanthanide elements (from La to Lu) plus the elements of yttrium (Y) and scandium (Sc). The trivalent lanthanide ions possess a $4f^n 5s^2 5p^6$ electronic structure with 14 available orbitals ($0 < n < 14$), offering 14 possible electronic group configurations. The quantum interaction of involved electrons endows lanthanide elements with abundant energy levels covering a spectral range of NIR, visible and ultraviolet (UV) (from 300 nm to 2500 nm)[50-54]. In addition, the perfect shielding of $4f$ electrons by outer complete $5s$ and $5p$ shells enables electronic transitions to occur with limited influence from the surrounding environment, thus exhibiting high resistance to processes of photo-bleaching. As the symmetries of involved quantum states are identical, the intra- $4f$ electronic transitions of lanthanide ions are electric-dipole forbidden, yet can be relaxed due to local-crystal-field-induced intermixing of the f states with higher electronic configurations. The primary forbidden nature yields metastable energy levels of lanthanide ions (lifetime can be as long as tens of milliseconds), thus favoring the occurrence of sequential excitations in excited states of a single lanthanide ion as well as permitting favorable ion-ion interactions in excited states to allow energy transfers between two or more lanthanide ions[29].

There are four main basic mechanisms for rare-earth ions based upconversion processes, given as:

1. Excited state absorption (ESA)
2. Energy transfer upconversion (ETU)
3. Photon avalanche (PA) and
4. Energy migration-mediated upconversion (EMU)

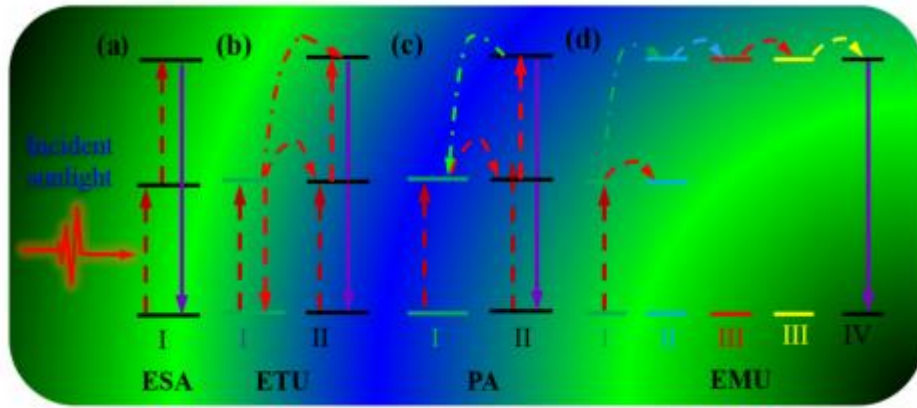


Fig 3.2: A schematic illustration of four typical upconversion processes: (a) Excited state absorption (ESA); (b) Energy transfer upconversion (ETU); (c) Photon avalanche (PA); (d) Energy migration-mediated upconversion (EMU).

3.3.1 Excited state absorption (ESA)

ESA takes the form of successive absorption of pump photons by a single ion utilizing the ladder-like structure of a simple multi-level system as portrayed in Fig 3.2 (a).

3.3.2 Energy transfer upconversion (ETU)

Fig 3.2 (a) illustrates a simplified three level system for two sequential photon absorption processes. The ETU process involves at least two types of ions, namely a sensitizer and an activator. In this process, ion I known as the sensitizer is firstly excited from the ground state to its metastable level by absorbing a pump photon; it then successively transfers its harvested energy to the ground state and the first excited state of ion II, known as the activator, exciting ion II to its upper emitting state, which is followed by radiative decay to its ground state.

3.3.3 Photon avalanche (PA)

The PA as shown in Fig 3.2 (c) is a looping process that involves an efficient cross relaxation mechanism between ion I in the ground state and ion II in the second excited state, resulting

in generation of two ion IIs in the metastable state. The population of ion II in the second excited state is created through absorption of laser photons at its metastable state (the first excited state), which is initially populated through non-resonant weak ground state absorption. When the looping process ensues, an avalanche population of ion II will be created at its metastable state, producing avalanche upconverted luminescence from the emitting state.

The generation of PA up-conversion typically occurs above a certain threshold of excitation density. Below the threshold, very little up-converted fluorescence is produced, while the luminescence intensity increases by orders of magnitude above the pump threshold. In addition, the looping nature enables the evoked up-conversion luminescence to be strongly dependent on the laser pump power, especially around the threshold laser power.

3.3.4 Energy migration-mediated upconversion (EMU)

The lanthanide ions designed for realizing energy migration-mediated upconversion (EMU) comprise four types: the sensitizers (type I), the accumulators (type II), the migrators (type III), and the activators (type IV; **Fig 3.2 (d)**). A sensitizer ion is used to harvest excitation photons and subsequently promotes a neighboring accumulator ion to its excited states. A migrator ion extracts the excitation energy from high-lying energy states of the accumulator, followed by random energy hopping through the migrator ion sub-lattice and trapping of the migrating energy by an activator ion that produces luminescence by decaying to the ground state.

3.4 Host Materials

Rare-earth-doped upconversion materials typically consist of an appropriate dielectric host matrix and doped Ln^{3+} ions that are dispersed as the guest in the lattice of the host matrix. Host materials with low phonon energy are able to produce upconversion luminescence at high efficiency, as multi-phonon-assisted non-radiative relaxations between the closely spaced energy levels can be minimized, thus yielding increased lifetime of intermediate energy levels. Investigated low phonon energy host materials typically include fluorides, chlorides, iodides, and bromides [55], while high phonon energy host materials such as silicates, borates, and phosphates are also under study [56].

In particular, hexagonal NaYF₄ lattice is considered to be one of the most efficient host materials to date [57-59]. Interestingly, even for cubic phase NaYF₄, a well-defined distribution of Na⁺ and Y³⁺ ions in the crystal lattice can enable ultrahigh upconversion luminescence [60]. The Ln³⁺ dopants provide light harvesting ability as well as upconverting ability for RED UC.

Among Ln³⁺ ions, the research for enhancing the efficiency of solar cells explores the use of single Ln³⁺ doping such as Er³⁺, Ho³⁺, Tm³⁺, and Pr³⁺ to upconvert IR light. Meanwhile, a utilization of Yb³⁺ ions as co-dopants can provide new, strong absorption at ~980 nm (2F_{7/2} → 2F_{5/2}). The Yb³⁺ ions are able to sensitize most lanthanide activator ions, typically, Er³⁺, Ho³⁺, Tm³⁺, resulting in intense upconversion when excited.

Table 3.1 summarizes some selected upconverting materials which can be excited, utilizing light with wavelength longer than 800 nm.

Dopant Ion	Host Material	Excitation (nm)	Emission (nm)
Er ³⁺	NaYF ₄	1523	550, 660, 800, 980
Yb ³⁺ -Er ³⁺	NaYbF ₄	980	520, 540, 654
Yb ³⁺ -Er ³⁺	NaYF ₄	980	410, 522, 540, 650
Yb ³⁺ -Er ³⁺	NaYF ₄ @NaYF ₄	980	510~570, 640~680
Yb ³⁺ -Er ³⁺	NaYF ₄ @NaYF ₄ :Nd ³⁺	808/980	520, 540, 655
Yb ³⁺ -Tm ³⁺	NaYF ₄	980	375, 450, 475, 679, 800
Yb ³⁺ -Ho ³⁺	NaYF ₄	980	545, 650
Yb ³⁺ -Er ³⁺ -Nd ³⁺	NaYF ₄	808/980	410, 520, 545, 650

1. Single Er³⁺ doped UC materials can convert light at 1523 nm to green (550 nm) and red (650 nm) (Fig 3.3 (a)) [61];
2. Yb³⁺/Er³⁺ co-doped system can produce green (525 nm, 542 nm), red (655 nm), as well as purple (415 nm, weak) emissions under 980 nm laser excitation [62];
3. Yb³⁺/Tm³⁺ pairs are able to convert light at 980 nm into UV (345 nm), blue (480 nm) and NIR (800 nm) emissions [63];
4. Nd³⁺/Yb³⁺/Ln³⁺ (Ln = Er, Tm, Ho, *etc.*) tri-doped UC materials can convert 808 nm NIR light to visible luminescence [64].

As an example, the energy transfer processes for Nd³⁺, Yb³⁺, and Er³⁺ are depicted in Fig 3.3 (b) for illustration. The Er³⁺ ion emits in the green and red range after absorbing the excitation energy by either the Nd³⁺ or the Yb³⁺ ions. Simultaneous use of Nd³⁺, Yb³⁺ and

Er³⁺ ions enables light harvesting at ~800 nm, ~980 nm, as well as ~1523 nm, covering broader spectral range for upconversion.

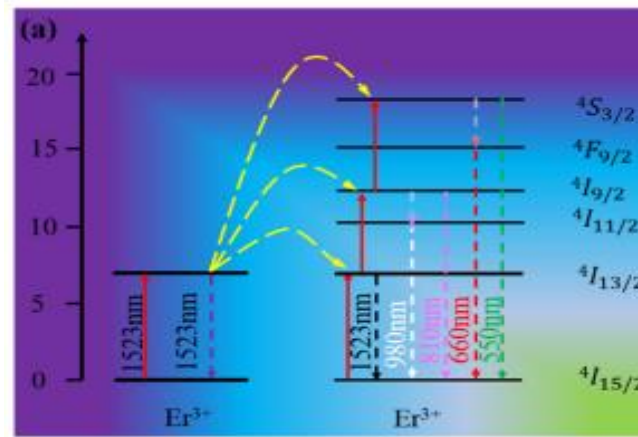


Fig 3.3 (a): The upconversion mechanisms for single Er³⁺ doped upconversion particles (UCNPs) excited under 1523 nm laser excitation.

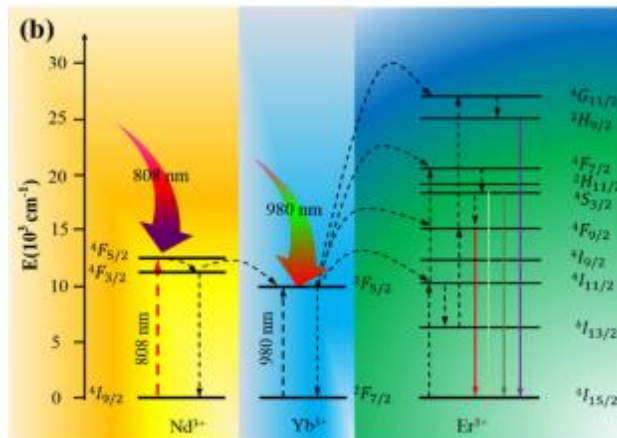


Fig 3.3 (b): The upconversion mechanisms for Nd³⁺-Yb³⁺-Er³⁺ tri-doped system under 808 nm or 980 nm laser excitation.

Chapter 4

Ag as Nanoparticle Material

There are a large number of metals available in nanoparticles form and that can be used in plasmonic solar cells. To find out the best suitable material to fulfill our purpose of higher quantum efficiency for solar cells Mie scattering simulations are performed.

The Mie scattering simulations are done using the software Lumerical FDTD Solutions. The software provides a powerful scripting language and graphical user interface environment. The scattering and absorption cross section can also be defined as

$$1. \quad \sigma_{scat}(\omega) = \frac{P_{scat}(\omega)}{I_{source}(\omega)}$$

$$2. \quad \sigma_{abs}(\omega) = \frac{P_{abs}(\omega)}{I_{inc}(\omega)}$$

Respectively. $P_{scat}(\omega)$ is the total scattered power, $I_{inc}(\omega)$ is the incident intensity and $P_{abs}(\omega)$ is the total power absorbed by the particle.

A spherical particle with 50nm radius is used for the simulation. A total field scattered field source covers a wavelength range of 300 to 600 nm is used is used for the plane wave excitation. Outside the TFST only the scattered fields are available. The monitor located outside the source will record the power scattered by the particles. The total fields are available in the region inside the source contain both the incident and scattered radiation. The absorbed field is calculated by subtracting the incident radiation from the total field outside of the source boundaries.

1. Absorption Cross Section

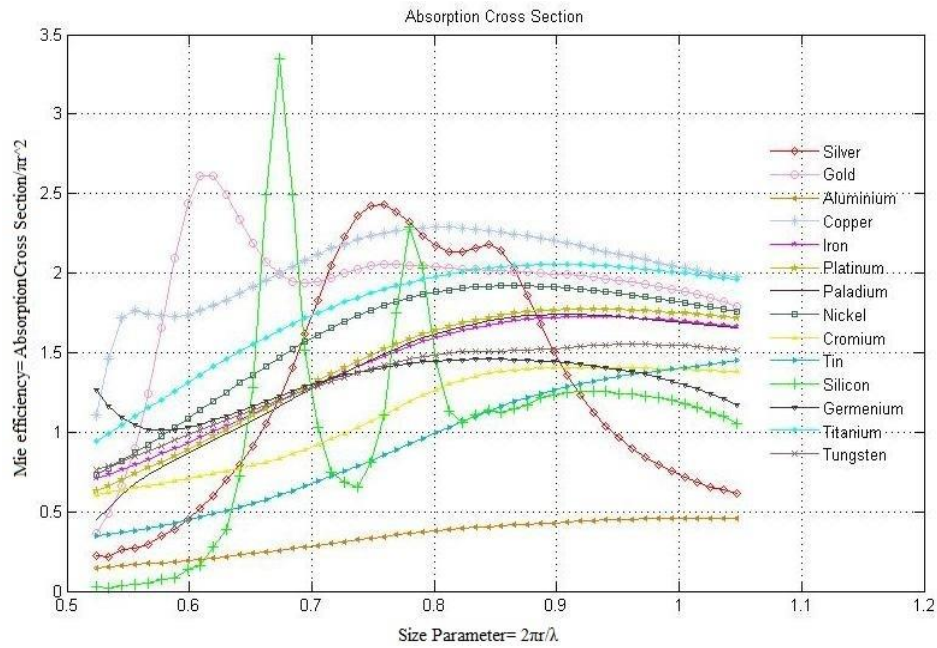


Fig 4.1: Absorption Cross Section of different spherical metallic nanoparticle vs size parameter

2. Scattering Cross section

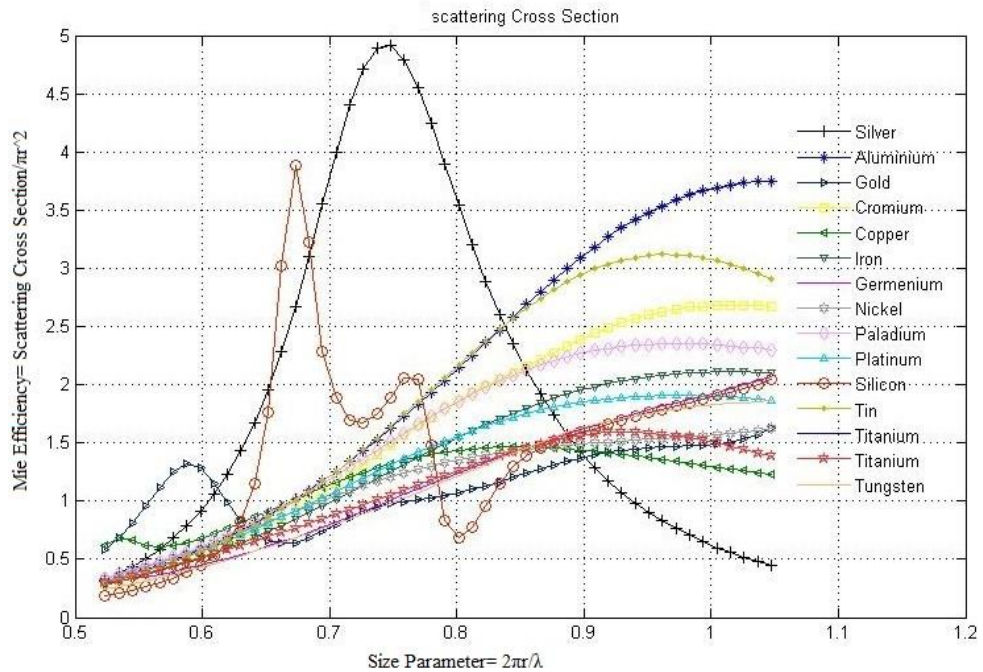


Fig 4.2: Scattering Cross Section of different spherical metallic nanoparticle vs size parameter

3. Fraction of total radiation scattered

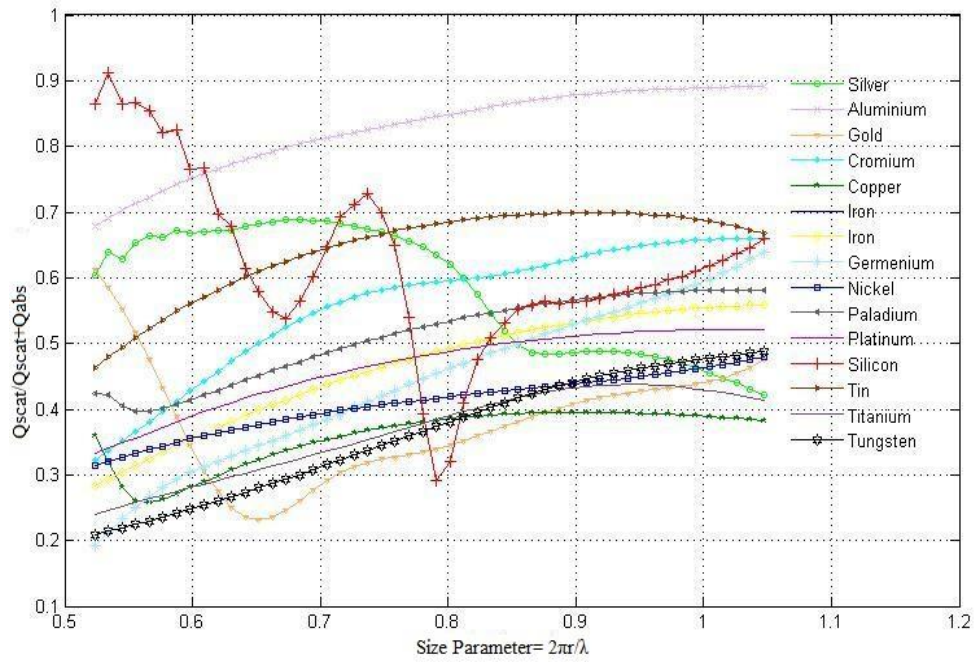


Fig 4.3: Fraction of scattering cross-section to the extinction cross-section of different spherical metallic nanoparticle versus size parameter

The Mie efficiencies for absorption and scattering are defined as:

$$Q_{abs} = \sigma_{abs}/\pi r^2$$

$$Q_{sca} = \sigma_{sca}/\pi r^2$$

Respectively, where σ_{abs} is the absorption cross-section given by the rate at which the energy is absorbed by the particle upon incident irradiance and σ_{sca} is defined as the scattering cross-section given by the rate at which energy is scattered upon the incident irradiance.

The Mie efficiencies for absorption and scattering are plotted as a function of size parameter of the nano particles. The solar irradiance is not uniformly distributed; rather it has a distribution centred on 500 nm wavelength region. The preferred particle should show maximum scattering in this range of wavelength. In order to find the best material for scattering applications the solar irradiance spectrum is integrated over wavelength from 300 nm to 600 nm with scattering efficiencies of particles as weight.

Table 4.1: The Scattering efficiency of different materials over broad spectrum of wavelength

The Scattering efficiency of different materials over broad spectrum of wavelength. $S(\lambda)$ is the solar spectral irradiance and $Q(\lambda)$ is the Mie efficiency of scattering

Material	$\int S(\lambda) * Q(\lambda)$	$\int S(\lambda) * Q(\lambda) / \int S(\lambda)$
Ag	668.8061785	1.973220951
Si	409.34592	1.207719025
Al	369.994862	1.091619122
Sn	363.0654496	1.071174841
Pd	339.061217	1.000353643
Au	325.814931	0.961272292
Cr	322.4639139	0.951385575
Cu	321.1998332	0.947656078
Pt	297.8905314	0.878885179
Fe	283.714159	0.837059735
Ni	283.204964	0.835557425
Ti	252.4476313	0.744812131
Ge	239.0700206	0.705343324
W	232.10887	0.684805404

Silver shows maximum integrated scattering efficiency of 1.973. From the data obtained, it can be concluded that silver is the best material for scattering light, followed by silicon and aluminium. Silver and gold are extensively used for plasmonic scattering application in thin film solar cells. But Silicon and Aluminium are showing reasonable scattering efficiencies. These materials can be used to replace expensive metals such as gold and silver. Silicon particles have added advantage that it reduces the problem of recombination, which is a major issue while using the metallic particles. The scattering efficiency of the particles can be further increased by optimizing the particle parameters such as size, shape, etc.

The magnitude of scattering depends upon the radius of the particle; hence there exists an optimum radius at which maximum scattering occurs. The variation of Mie efficiency for

different radii is plotted against broad spectrum of wavelength in order to figure out the optimal radius for scattering applications.

Variation of Scattering Efficiency with radius of Particles

In the case of Aluminum particles, an increase in radius results in a direct increase in both absorption and scattering efficiency. When calculating the fraction of total power scattered, the trend observed is, As the radius increases, the scattering efficiency also increases. We considered the radius ranging from 10nm to 70nm and found that the highest fraction of power scattered was that in the case of 70nm.

Similar trends are observed in the case of Silicon and Silver. The fraction of scattering for different radii peaks at different wavelengths. So depending upon the requirement of the application the scattering profile of the particle can be tuned by choosing the appropriate radii. In the case of Silver, higher scattering efficiency for wavelengths larger than 500nm is achieved by 70nm radius. The fraction of scattered power approaches unity in the range from 500nm to 700nm. The scattering cross section of Si particles is showing multiple peaks at various wavelengths for each of the radii. The peak value increases with increasing radius. Silicon scatters more in those wavelengths at which it exhibits weak absorption. This property can be exploited. Silicon nanoparticles can be used to scatter light into the silicon substrate which scatters more efficiently in the weakly absorbing regimes of the substrate.

Chapter 5

Proposed solar cell design

A. Krishnan [12] proposed a solar cell design using nanoparticle layers in both the surface and inside the bulk of the amorphous silicon. The perspective view of this design is as shown in the figure:

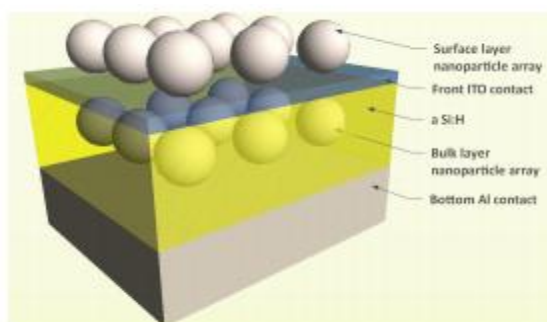


Fig 5.1: Perspective view of the solar cell with silver nanoparticle arrays on the surface and in the bulk [12].

In this solar cell the active region is made of amorphous silicon having a thickness of $0.3 \mu\text{m}$. Spherically shaped silver nanoparticles are placed periodically in rectangular arrays on the surface as well as inside the active region of the substrate. Particle layers are placed in such a way that nanoparticles in both layers are vertically aligned.

The various parameters of this solar cell are as shown in the figure below:

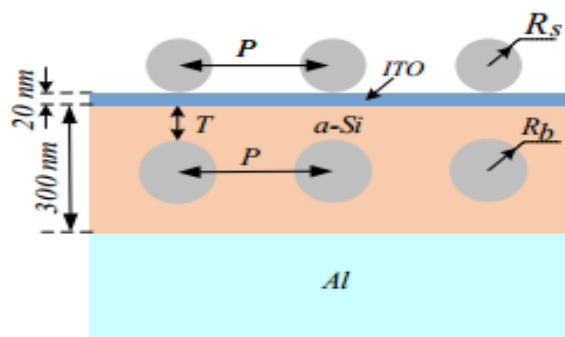


Fig 5.2: Various parameters.

The radius of the nanoparticles on the surface and in the active region are denoted by R_s and R_b respectively. The period of the nanoparticle array is denoted by P and the distance from the surface of the solar cell to the top of the bulk array is denoted by T . A 300 nm thick active region of amorphous silicon with an Aluminum back contact and a 20 nm thick ITO front contact is employed.

This solar cell is simulated for four possible designs.

Design 1

Considered as the primary reference, contains only the a-Si layer and does not incorporate any nanoparticle arrays for light trapping.

Design 2

It contains silver nanoparticle arrays on top of the ITO layer.

Design 3

A silver nanoparticle array is introduced into the bulk of the amorphous silicon.

Design 4

It corresponds to structure where nanoparticle arrays are introduced both in surface and bulk of the device.

Quantum efficiency

Quantum efficiency are calculated for all the designs considered [12]. The quantum efficiency of a solar cell for a particular wavelength, $QE(\lambda)$, is defined as the ratio of the absorbed power within the solar cell, $P_{abs}(\lambda)$, to the incident power of light, $P_{in}(\lambda)$.

$$QE(\lambda) = \frac{P_{abs}(\lambda)}{P_{in}(\lambda)}.$$

Quantum efficiency of these 4 designs are compared in the below figure

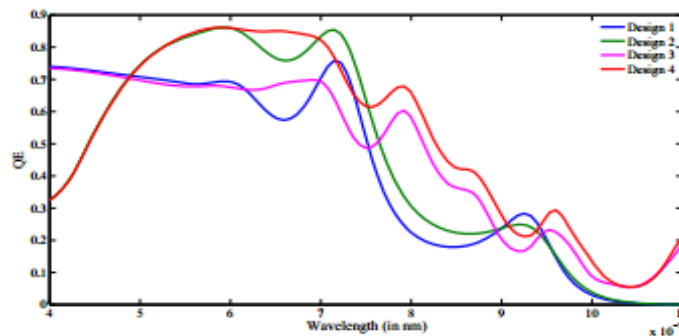


Fig 5.3: Quantum efficiency of various designs under consideration as a function of wavelength of light.

It can be observed that the design that employs nanoparticles on the surface and active region of the solar cell shows significant improvement in absorption efficiency over the reference designs. The introduction of nanoparticles on the surface improves the absorption efficiency of a-Si for a range of wavelengths between 500 *nm* and 900 *nm*, but causes little improvement at higher wavelengths. On the other hand, the introduction of nanoparticles inside the active region results in significant improvement in the absorption efficiency at most wavelengths above 620 *nm*, even though it has minimal effect at lower wavelengths.

This design exploits the absorption enhancement caused by both layers and produces improved absorption at all wavelengths. Around 620 – 900 *nm*, the simultaneous resonance from particles in both the layers enhances the field in the active region. The inter-layer particle interaction produces an improvement in photon absorption when compared to the enhancements caused by individual layers. The decrease in absorption efficiency below 500 *nm* for designs 2 and 4 is due to the screening effect caused by the nanoparticle layer on the surface of the device.

The plasmonic enhancement of the surface layer particles is negligible at these wavelengths and it prevents most of the incoming light from penetrating into the substrate. The introduction of nanoparticles on the bulk reduces the enhancement due to bottom metallic contact which results in a superior performance for Design 1 and 2 over the proposed device around wavelengths 720 *nm* and 940 *nm*.

Total Quantum efficiency

For the broad spectrum of incident electromagnetic radiation, the total quantum efficiency, TQE which takes the solar spectral irradiance into account, determines the overall absorption efficiency of the solar cell. TQE is the fraction of incident photons that are absorbed by the solar cell.

$$TQE = \frac{\int_{\lambda_1}^{\lambda_2} \frac{\lambda}{hc} QE(\lambda) I_{AM1.5}(\lambda) d\lambda}{\int_{\lambda_1}^{\lambda_2} \frac{\lambda}{hc} I_{AM1.5}(\lambda) d\lambda}$$

where h is Planck's constant, c is the speed of light in the free space and $I_{AM1.5}$ is the AM 1.5G solar spectrum. TQE and absorption enhancement for the broad spectrum of light as compared to the plain reference silicon solar cell are listed in following table.

Table 5.1: Comparison of TQE of the proposed design with the other considered designs and their enhancement as compared to a-Si without nanoparticles

Design	TQE (%)
Design 1	43.71
Design 2	49.09
Design 3	49.21
Design 4	56.01

5.1 Proposed design

Proposed design uses the same structure as proposed by A. Krishnan [5] with addition of a lanthanide layer i.e. (NaYF₄ with Er³⁺ doping) at depth of 40 nm from the surface and is 20 nm thick. The proposed design is as shown in the figure:

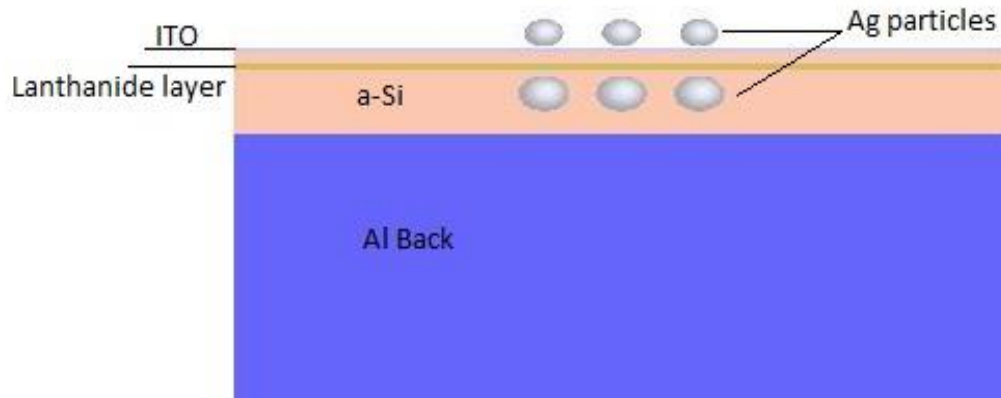


Fig 5.4: Proposed solar cell design with a lanthanide layer inside the bulk.

Initially the radii of the nanoparticles on the surface (R_s) and in the active region (R_b) are chosen as 50 nm and 65 nm respectively. The purpose is to exploit the plasmonic enhancement provided by different layers at different wavelength regimes so as to enhance the absorption over a wide band of wavelengths. The nanoparticles on the surface resonates at lower wavelengths and provides plasmonic enhancement in these regions. On the other hand the particle layer in the bulk with nanoparticles of higher size resonates at higher wavelengths and provide plasmonic enhancement in these wavelengths. In order to allow horizontal and vertical coupling of light between the nanoparticles, the period of the

nanoparticle arrays (P) is taken as 200 nm and the distance from the surface of the solar cell to the top of the bulk array (T) is taken as 85 nm. And thickness of lanthanide layer is taken as 20 nm.

The three dimensional finite difference time domain analysis (FDTD) tool provided by Lumerical is used for the design simulation. The amorphous silicon material is optically modeled using the refractive index data provided in the SOPRA N&K Database [65]. A normally incident plane wave source of unit amplitude with a wavelength range from 400 nm to 1100 nm is placed above the surface nanoparticle layer.

Periodic boundary conditions are used for the side boundaries to model the periodic nature of the particles. The Perfectly Matched Layer (PML) boundary conditions are used for upper and lower boundary to approximate the effect of infinite space and infinite bottom contact respectively. Mesh size of 2 nm is used for the regions where the particles are present and 3 nm for the a-Si absorber region.

The absorbed power within the active region of the solar cell is calculated with the help of 3-D power monitors placed on the a-Si substrate. The monitors record field data over the entire volume of the substrate and find the power absorbed as a function of spatial co-ordinates. For the design with particles embedded in the bulk, the power absorbed by the particles has to be deducted from the net absorbed power, since it does not contribute to the electron-hole pair generation. The power absorbed by the silicon absorber layer is calculated by applying a spatial filter which integrates the absorption within the filter region (here the a-Si substrate). The quantum efficiency and total quantum efficiency are calculated for all the designs considered.

5.2 Results

Here, quantum efficiency versus wavelength curves for a spectrum of 400 to 1100 nm are discussed. Results here shows that insertion of lanthanide layer inside the bulk of active region increases the absorption efficiency and hence the overall quantum efficiency.

Design 1

Following figure gives the quantum efficiency for a simple silicon cells with lanthanide layer without any surface and bulk nanoparticle layers.

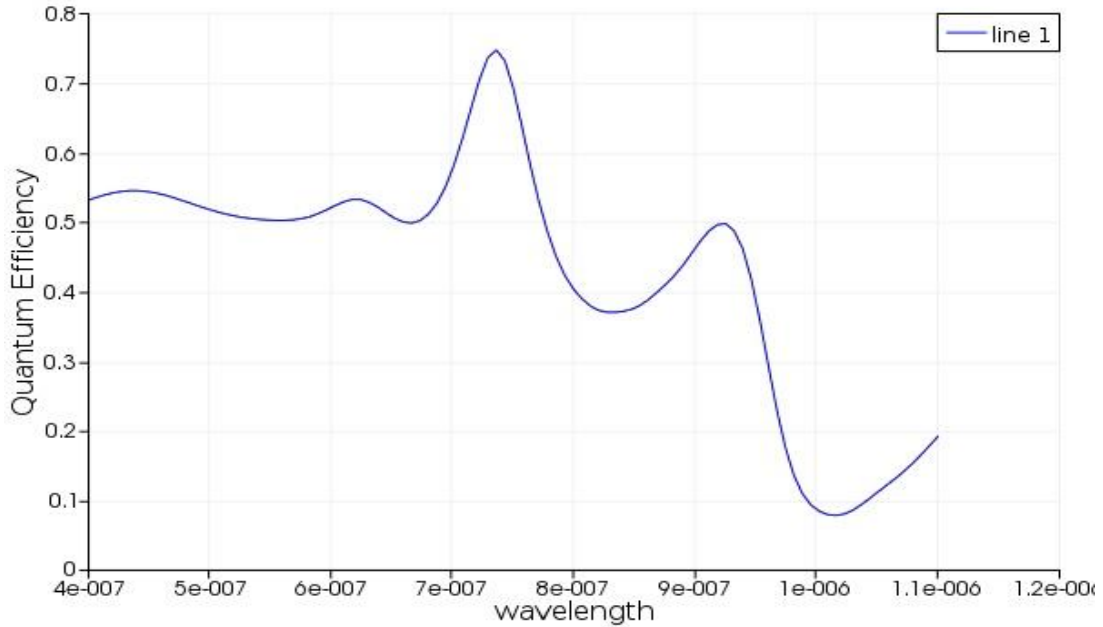


Fig 5.5: Quantum efficiency vs wavelength plot for proposed design without surface and bulk nanoparticles

It is evident from the graph that there is improvement in absorption in active region at wavelength of around 920 nm, this is because of the insertion of lanthanide layer inside the bulk of silicon. And the total quantum efficiency for this structure is found out to be 44.15%.

Design 2

Quantum efficiency for a structure with only surface nanoparticle layer is as shown in fig 5.6: It can be concluded from the figure that quantum efficiency at lower wavelengths is same as that of structure proposed by A. Krishnan [12] in his design 2. But there is a small improvement at higher wavelengths in quantum efficiency. Hence there is a small improvement in total quantum efficiency over design without lanthanide layer and is 51.34%.

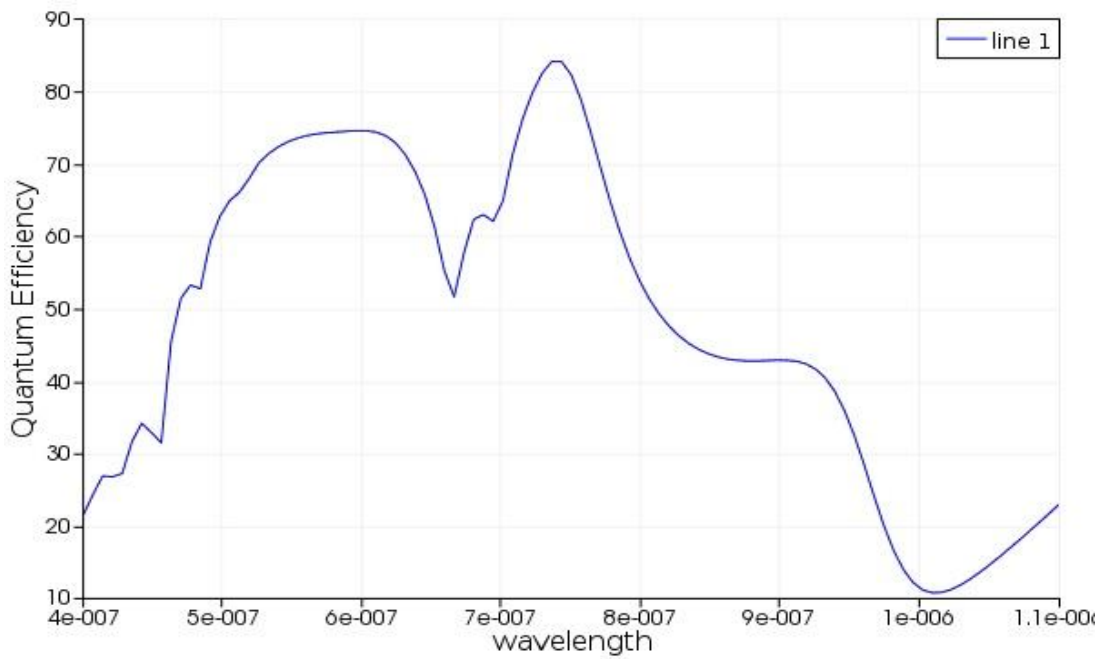


Fig 5.6: Quantum efficiency vs wavelength plot for proposed design with surface nanoparticle

Design 3

Quantum efficiency for a structure with only surface nanoparticle layer is as shown in fig 5.7:

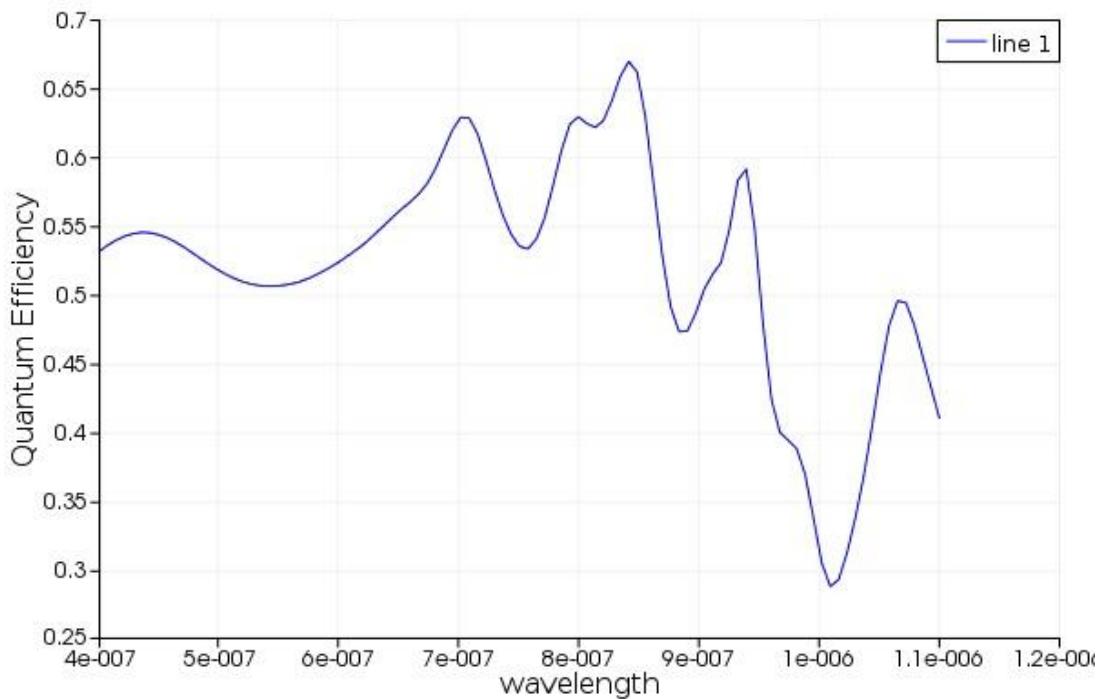


Fig 5.7: Quantum efficiency vs wavelength plot for proposed design with only bulk layer nanoparticles

It can be observed that there are peaks in value of quantum efficiency at wavelengths of around 840 nm and 950 nm. These peaks are because of the excitation of electrons from higher wavelengths to these wavelengths by the process of upconversion. These peaks contribute to the higher absorption at larger wavelengths. And total quantum efficiency for this structure is found out to be 52.61%, which is about 2% higher than the same structure without incorporation of lanthanide layer.

Design 4

This design consists of both the surface layer nanoparticles and the bulk layer nanoparticles along with the lanthanide layer for upconversion which is inserted in the bulk of the silicon active region. The quantum efficiency plot is as given in fig 5.8.

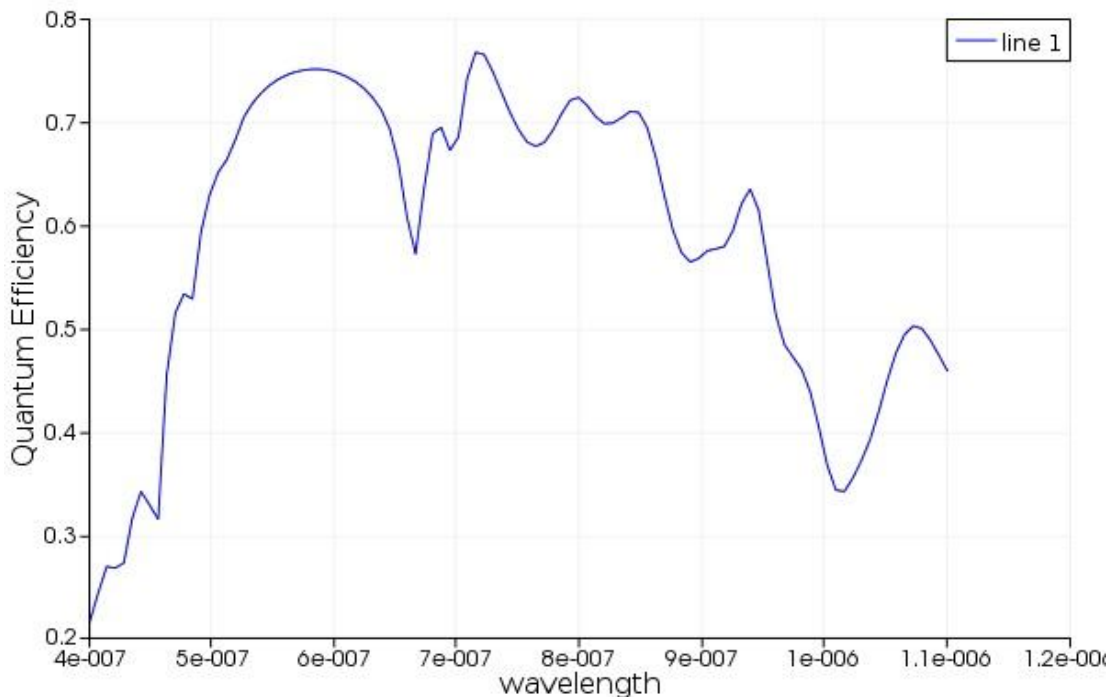


Fig 5.8: Quantum efficiency vs wavelength plot for proposed design with both the surface and bulk nanoparticle layers.

It is evident that we proposed design gives very good overall response for quantum efficiency by increasing the absorption of light in both the lower wavelength region and in the higher wavelength region. Broadening of spectrum in the wavelengths is accounted by the presence of upconversion layer in the bulk. Also there is a significant improvement at higher wavelengths in quantum efficiency as compared to the design without the lanthanide or

upconversion layer. Total quantum efficiency for the proposed design is 60.99 % showing an improvement of 4.98% over the design which do not incorporate any upconversion layer.

Total quantum efficiency (TQE) for all these 4 design is as summarized in the following table:

Table 5.2: Comparison of TQE of the proposed design with the other considered designs and their enhancement as compared to a-Si without nanoparticle and without upconversion layers

Design	TQE (%)
Design 1	44.15
Design 2	51.34
Design 3	52.61
Design 4	60.99

Chapter 6

Design parameters and their effects

Motive of this thesis is to have larger values of quantum efficiency for solar cells by using nanoparticles layers in the bulk i.e. active region and on the surface of the cell. There are various design parameters which influence the absorption profile of the thin film silicon substrate. There are three major parameters which effect the absorption profile.

1. Radii of nanoparticles
2. Particle layer separation and
3. Vertical alignment of particle layers

Surface plasmon resonance frequency is effected by change in the particle radius whereas the mutual interaction between the nanoparticle layers is affected by a change in particle layer separation as well as the alignment of particles in both the arrays. In detail study of these parameter variations influencing absorption efficiency of thin film substrate is as follows:

These results and variation effects are for the structure having amorphous silicon substrate of thickness having amorphous silicon substrate of thickness $0.3\mu\text{m}$. Spherical nanoparticles are periodically placed in rectangular arrays on the surface and inside the active region of the cell. $0.3\mu\text{m}$ silicon substrate is accompanied with an aluminum back contact and and a 20 nm thick indium-tin-oxide (ITO) front contact. Effect of parameter variations on quantum efficiency and total quantum efficiency of this structure are also studied.

6.1 Effect of nanoparticle radii

Both radii of surface layer nanoparticles (R_s) and bulk layer nanoparticle (R_b) effects the overall absorption efficiency. So, influence of change in particle radii for both surface and bulk is studied separately.

6.1.1 Effect of radii of surface layer nanoparticle (R_s)

The radius of surface nanoparticles (R_s) is varied from 0 nm to 100 nm and all the other design parameters are kept constant. Variation in R_s effects the frequency at which surface plasmon resonance will occur. The variation in quantum efficiency with change in R_s is as shown in the figure:

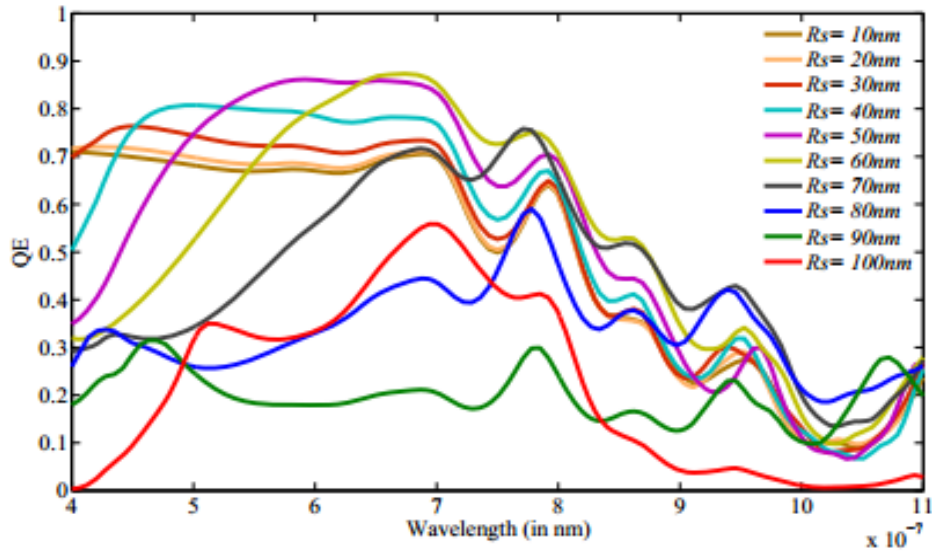


Fig 6.1: Variation of QE with wavelength for different surface layer particle radii.

From figure it can be interpreted that the magnitude of the absorption peak increases when the R_s increases from 0 nm to 60 nm. On further increasing R_s value reduction in magnitude of absorption peak is observed in the same wavelength range. Also for wavelength smaller than 750 nm the absorption peak shifts towards right with increase in particle radii. Another peak in QE is observed at lower wavelengths for R_s values greater than 70 nm.

As the particle size increases dynamic depolarization-on occurs because, conduction electrons across the particle no longer move in phase. This leads to a reduction in the depolarization field (which is generated by the surrounding polarized matter) at the centre of the particle. As a result, there is a reduced restoring force and hence a red-shift in the particle resonance. For particle sizes where scattering is significant, this re-radiation leads to a radiative damping correction to the quasi-static polarizability, the effect of which is to significantly broaden the plasmon resonance. The red-shift and broadening of the resonance with increased particle size would generally be expected to be an advantage for solar cell applications, since light-trapping should occur over a relatively broad wavelength range and at wavelengths that are long

compared with the quasi-static values of the surface plasmon resonance wavelengths of noble metal particles. While an increased size leads to a larger absolute scattering cross section, these effects do lead to a reduced cross section when normalized by size. Inclusion of dynamic depolarization and radiative damping effects can give reasonably accurate predictions of many features of the extinction spectra for larger particles for cases where the contribution of higher order multipoles can be neglected. It can be concluded that particle at surface mainly effects the absorption at lower wavelengths and has very little effect on absorption of higher wavelength radiations.

6.1.2 Effect of radii of bulk layer nanoparticle (R_b)

The radius of bulk nanoparticles (R_b) is varied from 0 nm to 100 nm and all the other design parameters are kept constant. The variation in quantum efficiency with change in R_s is as shown in the figure:

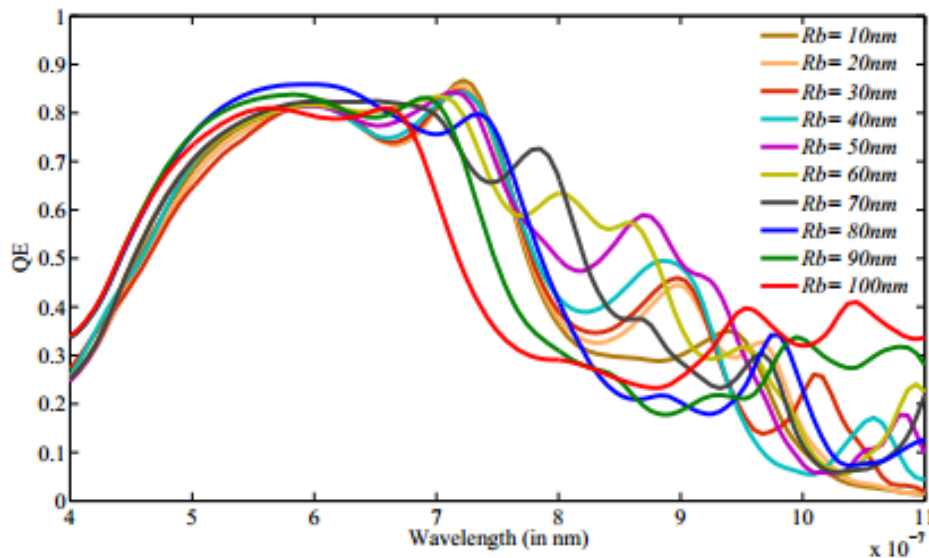


Fig 6.2: Variation of QE with wavelength for different bulk layer particle radii.

It is evident from the figure that particle in bulk layer do not significantly affect the absorption at lower wavelengths but have a notable effect at higher wavelength or lower energy radiations as when the light wave reaches bulk of the material some of the higher energy components loses their energy in form of absorption and scattering. The frequencies and intensities of localized surface plasmon resonances are known to be sensitive to the dielectric properties of the medium [66-68] and in particular, to the refractive index of matter close to

the particle surface. The larger particles show better absorption enhancement at higher wavelengths.

The effect of varying nanoparticle radii of bulk and surface layer towards the absorption of photons over the entire spectrum is shown in figure:

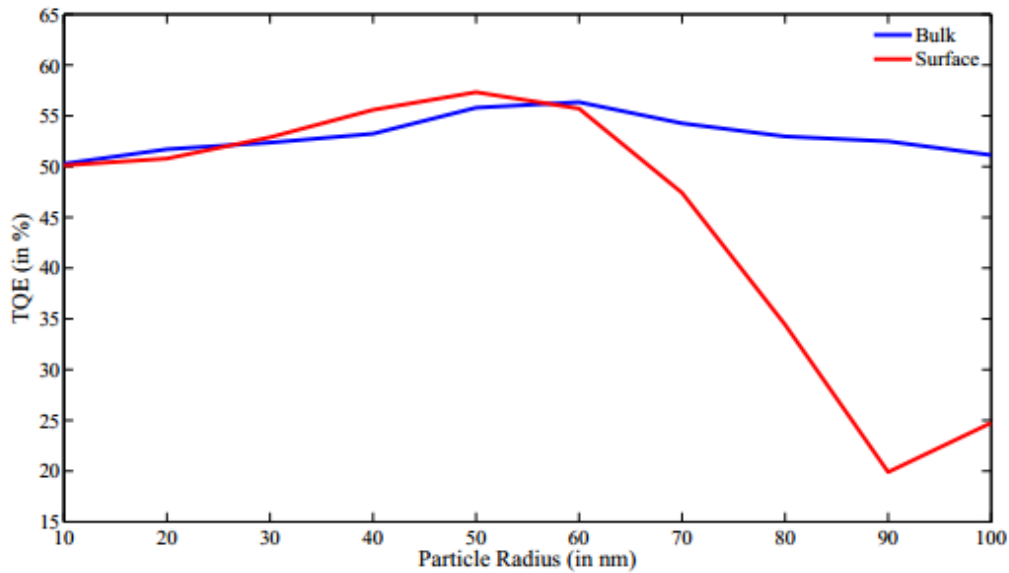


Fig 6.3: Variation in TQE with change in surface and bulk layer nanoparticle radii

It is evident from the graph that the surface layer radius variation affects the absorption to a higher extent. An initial increase in the radius of the surface layer nanoparticles causes an increment in Total Quantum Efficiency (TQE) but decreases when the particle radii exceeds 50 nm. Similarly, TQE increases with increase in R_b up-to 60 nm and then decreases with further increment in R_b .

6.2 Effect of particle layer separation

The distance of bulk nanoparticle layer from the surface layer effects the mutual interaction between the particle layers. The variation in absorption efficiency i.e. quantum efficiency as a function of wavelength as the inter particle layer separation (T: distance of bulk nanoparticle from silicon substrate surface) is varied from 17 nm to 153 nm is shown in the figure below. Inter particle distance is varied while keeping all other parameters i.e. substrate thickness 0.3

μm , period of nanoparticle array at 200 nm, radius of surface nanoparticle at 50 nm and radius of bulk nanoparticle at 65 nm.

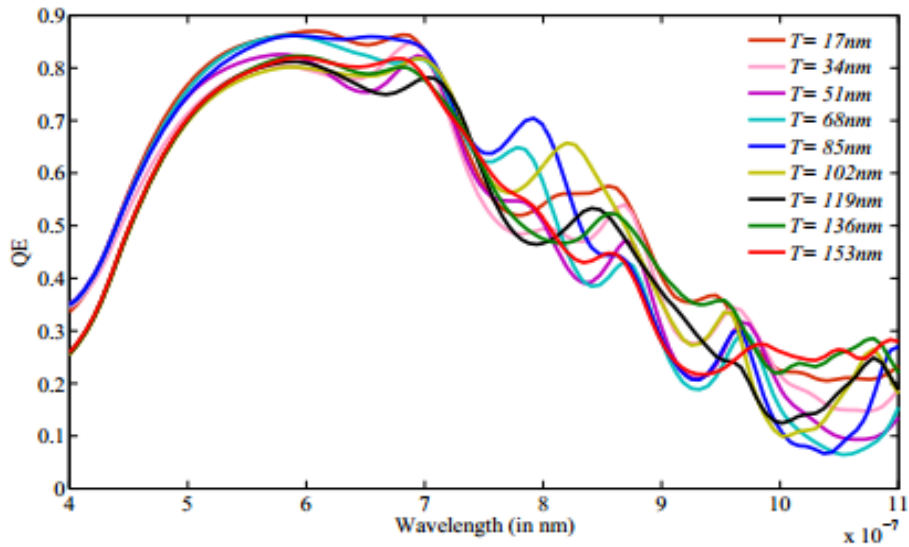


Fig 6.4: Variation of QE with change in inter particle layer separation

When the bulk nanoparticle layer is located near to the surface of amorphous silicon substrate then there is slight improvement in efficiency for wavelengths below 700 nm. Maximum absorption is observed when the nanoparticles in the bulk are located in the middle of the active region for wavelengths 700 nm to 800 nm. And for higher wavelengths i.e. greater than 850 nm there is better enhancement in absorption if the bulk nanoparticle layer is placed near bottom of the active region. Better observation can be made by looking at the total quantum efficiency measurement as shown below in the figure:

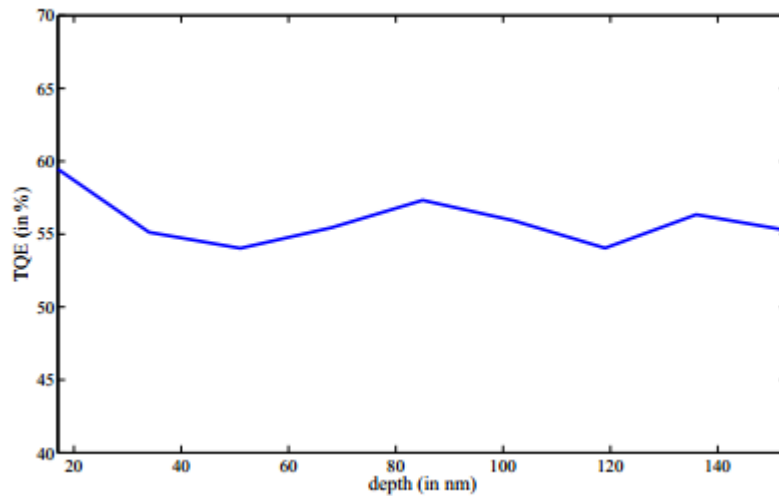


Fig 6.5: Variation of TQE with change in inter particle layer separation

It is evident that if the bulk nanoparticle layer is placed near to the surface there is increase in net absorption and hence better total quantum efficiency. There is a peak in TQE when the bulk nanoparticle layer is located near to the middle of the substrate and towards the bottom of the substrate. This is due to the absorption enhancement at these positions for wavelength range 700 – 800 nm and 850 – 1100 nm respectively. This implies that range of absorption for this structure is extended in the near infra-red (NIR i.e. wavelength range from 700 nm to 2500 nm) region.

6.3 Effect of vertical alignment of particle layers

Theoretical results are obtained by keeping both the surface nanoparticle layer and bulk nanoparticle layer that's id embedded in the a-Si substrate in perfect alignment. But practically perfect vertical alignment is very difficult to attain. To understand the extent to which the alignment of two nanoparticle layers affect the light absorption in the proposed design, the bulk array is moved in the horizontal direction while keeping the position of the surface array unaltered. The horizontal distance l between the centers of nanoparticles in both the layers is a measure of misalignment between the particle layers. The variation in absorption efficiency and total quantum efficiency when the bulk array is moved away from the normal is shown in figures:

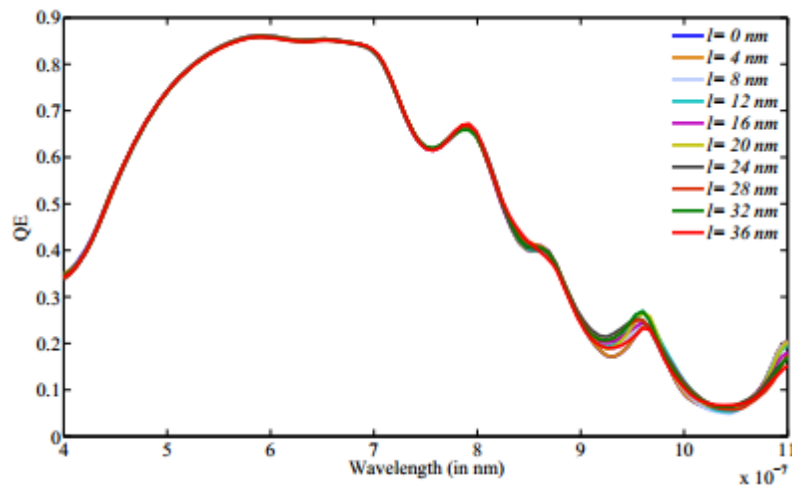


Fig 6.6: Variation of QE and with change in the alignment of particles.

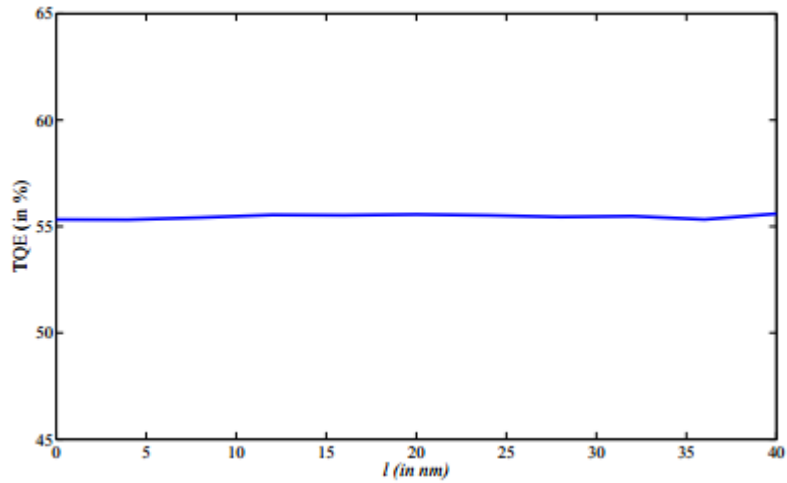


Fig 6.7: Variation of T QE with change in the alignment of particles.

The QE and TQE plot for various l values shows that there is very little change in absorption efficiency when the nanoparticles in the bulk array is moved horizontally away from the normal passing through the center of the top layer nanoparticles. A slight mismatch in vertical alignment of nanoparticle arrays does not affect the overall absorption. Therefore the constraint of perfect vertical alignment can be relaxed while placing nanoparticle arrays in the solar cell [12].

Chapter 7

Conclusion

The proposed solar cell design exploits the cumulative plasmonic enhancement from different nanoparticle layers at different wavelengths and improves the absorption efficiency over the entire range of wavelength. For calculating the short circuit current, recombination occurring in the device need to be considered. Recombination due to nanoparticles can be mitigated either by depositing nanoparticles at room temperature or by coating the nanoparticles with a thin dielectric layer.

Insertion of upconversion layer inside the bulk of the active region gives significant improving in total quantum efficiency by increasing the absorption efficiency mainly in the high wavelength region and broadening of quantum efficiency profile for lower and mid wavelength regions.

In summary, the theoretical study shows that the thin film amorphous silicon solar cell with presence of lanthanide layer (for upconversion process) along with nanoparticle arrays placed on the surface and in the semiconductor layer and showed significant improvement in absorption efficiency. The metallic nanoparticles at the surface contributes to the enhancement at lower wavelengths and those embedded within the absorber layer contributes to the enhancement at higher wavelengths. Also these is improvement in mid wavelength region due to the upconversion process. The inter layer particle interaction further enhances the field intensity at intermediate wavelengths. Therefore, the design put forward in this thesis exploits the surface plasmon resonance from metallic nanoparticles at all wavelengths and thus provides significant improvement in the overall light absorption efficiency.

References

- [1] L. Tsakalakos, “Nanostructures for photovoltaics,” *Mater. Sci. Eng. R Reports*, vol. 62, no. 6, pp. 175–189, 2008. E. Achenbach. Response of a solid oxide fuel cell to load change. *J. Power Sources* 57, (1995) 105–109.
- [2] K. R. Catchpole and a Polman, “Plasmonic solar cells.,” *Opt. Express*, vol. 16, no. 26, pp. 21793–800, 2008.
- [3] B. M. van der Ende, L. Aarts, and A. Meijerink, “Lanthanide ions as spectral converters for solar cells.,” *Phys. Chem. Chem. Phys.*, vol. 11, no. 47, pp. 11081–95, 2009.
- [4] E. Becquerel, *La lumi_ere: ses causes et ses e_ets*, tome second, Paris (1867), p. 122.
- [5] D.M. Chapin, C.S., Fuller, G.S. Pearson, A new silicon p–n junction photocell for converting solar radiation into electrical power, *J. Appl. Phys.* 25 (1954) 676.
- [6] J. Zhao, A. Wang, M.A. Green, F. Ferrazza, *Appl. Phys. Lett.* 73 (1998) 1991
- [7] W. Shockley, H.J. Queisser, *J. Appl. Phys.* 32 (1961) 510
- [8] M.J. Kerr, P. Campbetl, A. Cuevas, in: *Proceedings of the 29th IEEE Photovoltaic Specialists Conference*, New Orleans, (2002), p. 438.
- [9] H. A. Atwater and A. Polman, “Plasmonics for improved photovoltaic devices,” *Nat. Mater.*, vol. 9, no. 10, pp. 865–865, 2010.
- [10] J. Müller, B. Rech, J. Springer, and M. Vanecek, "TCO and light trapping in silicon thin film solar cells," *Solar Energy* 77, 917-930 (2004).
- [11] J. Meier, S. Dubail, S. Golay, U. Kroll, S. Faÿ, E. Vallat-Sauvain, L. Feitknecht, J. Dubail, and A. Shah, "Microcrystalline silicon and the impact on micromorph tandem solar cells," *Sol. Energy Mater. Sol. Cells* 74, 457-467 (2002).
- [12] A. Krishnan, S. Das, S. R. Krishna, and M. Z. Khan, “Multilayer nanoparticle arrays for broad spectrum absorption enhancement in thin film solar cells,” *Opt Express*, vol. 22 Suppl 3, no. 2012, pp. A800–11, 2014.
- [13] S. Pillai, K. R. Catchpole, T. Trupke, and M. A. Green, “Surface plasmon enhanced silicon solar cells,” *J. Appl. Phys.* 101, 093105 (2007)
- [14] W. L. Barnes, A. Dereux, and T. W. Ebbesen, “Surface plasmon subwavelength optics,” *Nature* 424, 824–830 (2003)

- [15] F. Bohren and D. R. Huffman, *Absorption and Scattering of Light by Small Particles* (Wiley-Interscience, 1983).
- [16] P. Spinelli, V. E. Ferry, J. van de Groep, M. van Lare, M. A. Verschuuren, R. E. I. Schropp, H. A. Atwater, and Polman, "Plasmonic light trapping in thin-film Si solar cells," *J. Opt.*14, 024002 (2012).
- [17] H. A. Atwater and A. Polman, "Plasmonics for improved photovoltaic devices," *Nat. Mater.*9, 205–213 (2010)
- [18] Y. A. Akimov and W. S. Koh, "Design of plasmonic nanoparticles for efficient subwavelength light trapping in thin-film solar cells," *Plasmonics*6, 155–161 (2011)
- [19] L. Chen, W. C. H. Choy, and W. E. I. Sha, "Broadband absorption enhancement of organic solar cells with interstitial lattice patterned metal nanoparticles," *Appl. Phys. Lett.*102, 251112 (2013)
- [20] S. Pillai, F. J. Beck, K. R. Catchpole, Z. Ouyang, and M. A. Green, "The effect of dielectric spacer thickness on surface plasmon enhanced solar cells for front and rear side depositions," *J. Appl. Phys.*109, 073105 (2011)
- [21] H. Choi, J. P. Lee, S. J. Ko, J. W. Jung, H. Park, S. Yoo, O. Park, J. R. Jeong, S. Park, and J. Y. Kim, "Multipositional silica-coated silver nanoparticles for high-performance polymer solar cells," *Nano Lett.*13, 2204–2208(2013).
- [22] C.-I. Ho, D.-J. Yeh, V.-C. Su, C.-H. Yang, P.-C. Yang, M.-Y. Pu, C.-H. Kuan, I. C. Cheng, and S.-C. Lee, "Plasmonic multilayer nanoparticles enhanced photocurrent in thin film hydrogenated amorphous silicon solar cells," *J. Appl. Phys.*112, 023113 (2012).
- [23] Y. Shi, X. Wang, W. Liu, T. Yang, R. Xu, and F. Yang, "Multilayer silver nanoparticles for light trapping in thin film solar cells," *J. Appl. Phys.*113, 176101 (2013).
- [24] M. A. Sefunc, A. K. Okyay, and H. V. Demir, "Volumetric plasmonic resonator architecture for thin-film solar cells," *Appl. Phys. Lett.*98, 093117 (2011).
- [25] A. Lin, S.-M. Fu, Y.-K. Chung, S.-Y. Lai, and C.-W. Tseng, "An optimized surface plasmon photovoltaic structure using energy transfer between discrete nanoparticles," *Opt. Lett.*21, A131–A145 (2013).
- [26] R. Santbergen, R. Liang, and M. Zeman, "A-Si: H solar cells with embedded silver nanoparticles," in *Photovoltaic Specialists Conference (PVSC)*(2010), pp. 748.
- [27] M. Xue, L. Li, B. J. T. de Villiers, H. Shen, J. Zhu, Z. Yu, A. Z. Stieg, Q. Pei, B. J. Schwartz, and K. L. Wang, "Charge-carrier dynamics in hybrid plasmonic organic solar cells with Ag nanoparticles," *Appl. Phys. Lett.*98,253302 (2011).

- [28] V. Santhanam and R. P. Andres, "Microcontact printing of uniform nanoparticle arrays," *Nano Lett.* 4, 41–44 (2004).
- [29] Y. Shang, S. Hao, C. Yang, and G. Chen, "Enhancing Solar Cell Efficiency Using Photon Upconversion Materials," *Nanomaterials*, vol. 5, no. 4, pp. 1782–1809, 2015.
- [30] Zhang, X.D.; Jin, X.; Wang, D.F.; Xiong, S.Z.; Geng, X.H.; Zhao, Y. Synthesis of NaYF₄:Yb, Er nanocrystals and its application in silicon thin film solar cells. *Phys. Status Solidi C* 2010, 7, 1128–1131.
- [31] U. Kreibig and M. Vollme, *Optical Properties of Metal Clusters* (Springer-Verlag, 1995), vol. 25.
- [32] S. Zeng, K.-T. Yong, I. Roy, X.-Q. Dinh, X. Yu, and F. Luan, "A review on functionalized gold nanoparticles for biosensing applications," *Plasmonics* 6, 491–506 (2011)
- [33] K. R. Catchpole and A. Polman, "Plasmonic solar cells," *Opt. Express* 16, 21793–21800 (2008)
- [34] M. Meier and A. Wokaun, "Enhanced fields on large metal particles: dynamic depolarization," *Opt. Express* 8, 581–583 (1993).
- [35] J. P. Kottmann and O. J. F. Martin, "Retardation-induced plasmon resonances in coupled nanoparticles," *Opt. Lett.* 26, 1096–1098 (2001).
- [36] C. Dahmen, B. Schmidt, and G. von Plessen, "Radiation damping in metal nanoparticle pairs," *Nano Lett.* 7, 318–322 (2007).
- [37] G. Xu, M. Tazawa, P. Jin, S. Nakao, and K. Yoshimura, "Wavelength tuning of surface plasmon resonance using dielectric layers on silver island films," *Appl. Phys. Lett.* 82, 3811–3813 (2003)
- [38] S. Pillai, K. R. Catchpole, T. Trupke, and M. A. Green, "Surface plasmon enhanced silicon solar cells," *J. Appl. Phys.*, vol. 101, no. 9, pp. 1–8, 2007
- [39] W. G. van Sark, J. de Wild, J. K. Rath, A. Meijerink, and R. E. Schropp, "Upconversion in solar cells," *Nanoscale Res. Lett.*, vol. 8, no. 1, p. 81, 2013.
- [40] Van Sark WGJHM, Meijerink A, Schropp REI, Van Roosmalen JAM, Lysen EH: Enhancing solar cell efficiency by using spectral converters. *Sol En Mater Sol Cells* 2005, 2005(87):395–409
- [41] Trupke T, Green MA, Würfel P: Improving solar cell efficiencies by down-conversion of high-energy photons. *J Appl Phys* 2002, 92:1668–1674.
- [42] Trupke T, Green MA, Würfel P: Improving solar cell efficiencies by up-conversion of sub-band-gap light. *J Appl Phys* 2002, 92:4117–4122.

- [43] Richards BS:Enhancing the performance of silicon solar cells via the application of passive luminescence conversion layers.*Sol En Mater Sol Cells*2006,90:2329–2337.
- [44] Minemoto T, Toda M, Nagae S, Gotoh M, Nakajima A, Yamamoto K, Takakura H, Hamakawa Y:Effect of spectral irradiance distribution on the outdoor performance of amorphous Si//thin-film crystalline Si stacked photovoltaic modules.*Sol En Mater Sol Cells*2007,91:120–122.
- [45] Van Sark WGJHM:Simulating performance of solar cells with spectral downshifting layers. *Thin Solid Films*2008,516:6808–6812.
- [46] Auzel F:Upconversion and anti-stokes processes with f and d ions in solids.*Chem Rev*2004,104:139–173.
- [47] Strümpel C, McCann M, Beaucarne G, Arkhipov V, Slaoui A,Švrček V, del Cañizo C, Tobias I:Modifying the solar spectrum to enhance silicon solar cell efficiency - an overview of available materials.*Sol En Mater Sol Cells* 2007,91:238–249
- [48] Wang, F.; Banerjee, D.; Liu, Y.S.; Chen, X.Y.; Liu, X.G. Upconversion Nanoparticles in Biological Labeling, Imaging and Therapy. *Analyst* 2010, 135, 1839–1854.
- [49] Wang, F.; Liu, X.G. Recent advances in the chemistry of lanthanide-doped upconversion nanocrystals. *Chem. Soc. Rev.* 2009, 38, 976–989
- [50] Bunzli, J.C.G. Benefiting from the Unique Properties of Lanthanide Ions. *Acc. Chem. Res.* 2006, 39, 53–61.
- [51] Bunzli, J.C.G. Lanthanide luminescence for biomedical analyses and imaging. *Chem. Rev.* 2010, 110, 2729–2755.
- [52] Carlos, L.D.; Ferreira, R.A.S.; Bermudez, V.D.; Julian-Lopez, B.; Escribano, P. Progress on lanthanide-based organic-inorganic hybrid phosphors. *Chem. Soc. Rev.* 2011, 40, 536-549.
- [53] Kar, A.; Patra, A. Impacts of core-shell structures on properties of lanthanide-based nanocrystals: Crystal phase, lattice strain, downconversion, upconversion and energy transfe. *Nanoscale* 2012, 4, 3608–3619.
- [54] Goesmann, H.; Feldmann, C. Nanoparticulate Functional Materials. *Angew. Chem. Int. Ed.* 2010, 49, 1362–1395.
- [55] Ohwaki, J.; Wang, Y. Efficient 1.5mm to visible upconversion in Er³⁺ -doped halide phosphors. *Jpn. J. Appl. Phys.* 1994, 33, 334–337.
- [56] Auzel, F.; Pecile, D.; Morin, D. Rare earth doped vitroceraamics: New, efficient, blue and green emitting materials for infrared upconversion. *J. Electrochem. Soc.* 1975, 122,doi:10.1149/1.2134132.

- [57] Menyuk, N.; Dwight, K.; Pierce, J.W. NaYF₄:Yb,Er—An efficient upconversion phosphor. *Appl. Phys. Lett.* 1972, 21, 159–161.
- [58] Suyver, J.F.; Grimm, J.; Krämer, K.W.; Güdel, H.U. Highly Efficient Near-Infrared to Visible Up-Conversion Process in NaYF₄:Er³⁺,Yb³⁺. *J. Lumin.* 2005, 114, 53–59.
- [59] Krämer, K.W.; Biner, D.; Frei, G.; Güdel, H.U.; Hehlen, M.P.; Lüthi, S.T. Hexagonalsodium yttrium fluoride based green and blue emitting upconversion phosphors. *Chem. Mater.* 2004, 16, 1244–1251.
- [60] Wang, L.; Li, X.; Li, Z.; Chu, W.; Li, R.; Lin, K.; Qian, H.; Wang, Y.; Wu, C.; Li, J.; et al. A New Cubic Phase for a NaYF₄ Host Matrix Offering High Upconversion Luminescence Efficiency. *Adv. Mater.* 2015, 27, doi:10.1002/adma.201502748
- [61] Chen, G.Y.; Ohulchanskyy, T.Y.; Kachynski, A.; Agren, H.; Prasad, P.N. Intense Visible and Near-Infrared Upconversion Photoluminescence in Colloidal LiYF₄:Er³⁺ Nanocrystals under Excitation at 1490 nm. *ACS Nano* 2011, 5, 4981–4986
- [62] Li, C.; Lin, J. Rare earth fluoride nano-/microcrystals: Synthesis, surface modification and application. *J. Mater. Chem.* 2010, 20, 6831–6847.
- [63] Chen, D.; Zhou, Y.; Wan, Z.; Huang, P.; Yu, H.; Lu, H.; Ji, Z. Enhanced upconversion luminescence in phase-separation-controlled crystallization glass ceramics containing Yb/Er(Tm):NaLuF₄ nanocrystals. *J. Eur. Ceram. Soc.* 2015, 35, 2129–2137
- [64] Li, Q.; Lin, J.; Wu, J.; Lan, Z.; Wang, Y.; Peng, F.; Huang, M. Enhancing photovoltaic performance of dye-sensitized solar cell by rare-earth doped oxide of Lu₂O₃:(Tm³⁺,Yb³⁺). *Electrochim. Acta* 2011, 56, 4980–4984
- [65] <http://www.spectra.com/sopra.html>.
- [66] A. J. Haes, S. L. Zou, G. C. Schatz, and R. P. Van Duyne, “Nanoscale optical biosensor: short range distance dependence of the localized surface plasmon resonance of noble metal nanoparticles,” *J. Phys. Chem.* B108,6961–6968 (2004).
- [67] P. Hanarp, M. Kall, and D. S. Sutherland, “Optical properties of short range ordered arrays of nanometer gold disks prepared by colloidal lithography,” *J. Phys. Chem.* B107, 5768–5772 (2003).
- [68] T. R. Jensen, M. D. Malinsky, C. L. Haynes, and R. P. Van Duyne, “Nanosphere lithography: tunable localized surface plasmon resonance spectra of silver nanoparticles,” *J. Phys. Chem.* B104, 10549–10556 (2000)